Three-Dimensional Transient Electromagnetic Modeling Using Rational Krylov Methods

Börner, Ralph-Uwe and Ernst, Oliver G. and Güttel, Stefan

2014

MIMS EPrint: **2014.36**

Manchester Institute for Mathematical Sciences
School of Mathematics

The University of Manchester

Reports available from: http://eprints.maths.manchester.ac.uk/
And by contacting: The MIMS Secretary
School of Mathematics
The University of Manchester
Manchester, M13 9PL, UK

ISSN 1749-9097

Three-Dimensional Transient Electromagnetic Modeling Using Rational Krylov Methods

Ralph-Uwe Börner, Oliver G. Ernst, and Stefan Güttel

Thursday 18th December, 2014

SUMMARY
A computational method is given for solving the forward modeling problem for transient electromagnetic exploration. Its key features are the discretization of the quasi-static Maxwell's equations in space using the first-kind family of curl-conforming Nédélec elements combined with time integration using rational Krylov methods. We show how rational Krylov methods can also be used to solve the same problem in the frequency domain followed by a synthesis of the transient solution using the fast Hankel transform, and we argue that the pure time-domain solution is more efficient. We also propose a new surrogate optimization approach for selecting the pole parameters of the rational Krylov method which leads to convergence within an a priori determined number of iterations independent of mesh size and conductivity structure. These poles are repeated in a cyclic fashion, which, in combination with direct solvers for the discrete problem, results in significantly faster solution times than previously proposed schemes.

Key words: EM modeling, transient electromagnetics, rational Krylov methods

1 INTRODUCTION

The rapid numerical inversion and simulation of 3-D electromagnetic (EM) measurements to obtain maps of electromagnetic conductivity of subsurface regions of interest remains one of the major computational challenges of geoelectromagnetic prospecting. The *forward simulation* or *modeling* step, in which the response of a given conductivity distribution is computed, is a key element in the inversion process since it must be carried out multiple times for each inversion. The availability of fast forward modeling codes is therefore of crucial importance.

A broad distinction in EM forward modeling schemes is between *time-domain* and *frequency-domain* methods. In the first, the time evolution of electromagnetic fields is propagated forward in time, whereas in the latter the Fourier components of these fields are computed for a suitable collection of frequencies, which are then transformed numerically to the time domain. Both approaches are mathematically equivalent and, as we demonstrate below, can be implemented using rational Krylov methods; however, as will become clear, simpler and more accurate numerical methods for TEM forward modeling result when performing all calculations in the time domain.

The finite-difference time-domain (FDTD) scheme introduced by Yee (1966) based on staggered tensor product grids in space has been widely used to model responses of 2-D and 3-D conductivity structures by time-stepping (Taflove 1995). The Yee discretization combined with explicit and implicit time-stepping also forms the basis of transient electromagnetic modeling in the geophysics literature. Among these are Oristaglio and Hohmann (1984), where the 2-D problem of transient electromagnetics is solved with an explicit time-integration scheme proposed by DuFort and Frankel (1953) combined with an upward continuation boundary condition at the air-Earth interface. This approach was extended to model 3-D inhomogeneities in Wang and Hohmann (1993). Commer and Newman (2004) present a finite difference scheme for the simulation of transient electromagnetic fields generated by galvanic sources. They were able to compute the initial conditions by solving a stationary 3-D Poisson problem, as it appears, e.g., in the numerical solution of the 3-D DC resistivity problem. Moreover, their algorithm was designed to run on parallel computer architectures.

The stability constraints of explicit time-stepping schemes for the parabolic quasi-static Maxwell's equations require excessively small time steps for fine spatial resolution and low conductivities. Although each time step consists of essentially a matrix-vector product, small time steps can nonetheless lead to high computational demands. As demonstrated in Oristaglio and Hohmann (1984), the DuFort-Frankel scheme allows the time step to increase with the square root of simulation time as the integration progresses. However, the initial time step still depends on the smallest conductivity present in the model. Typical values for the choice of the air half-space conductivity range between 10^{-14} and 10^{-6} S/m.

Unlike explicit schemes, implicit methods solve a system of linear equations to obtain the solution for each desired time step. Goldman and Stoyer (1983) have simulated transients for 2-D structures with axial symmetry by implicit time-stepping. Haber et al. (2002) simulated 3-D transients employing a backward Euler scheme, a variant of the implicit time-stepping method. At each time step, they solved the system of linear equations arising from a finite volume discretization. The system was solved with a preconditioned biconjugate gradient method.

Transient electromagnetic fields may also be obtained by

inverse Fourier transformation of sufficiently many frequency-domain solutions. Newman et al. (1986) implemented an integral equation formulation in the frequency domain, and transformed the solutions back to the time domain using a fast Hankel transform. A similar approach was proposed by Mulder et al. (2008), who compute a small number of frequency-domain solutions and transform a spline-interpolated set of solutions to the time domain. The discrete times for which a transient can be calculated depend on the sampling interval as well as the bandwidth of the discrete solutions given in the frequency domain. Generally, for a transient spanning from very early to late times, e.g., from 10^{-6} to 10^{-3} seconds, many—typically around 100—frequency-domain solves are necessary, which requires an unreasonably high numerical effort.

Improvements over explicit or implicit time-stepping can be achieved using Krylov methods. Like time-stepping, polynomial and rational Krylov subspace methods for solving the quasi-static Maxwell's equations require a matrix-vector product or linear system solve, respectively, at each iteration step. However, the approximations at the desired time values are obtained by choosing a near-best approximation from a global Krylov space whose dimension increases with each Krylov iteration. For the frequency-domain approach the solution at the desired frequencies required for Fourier synthesis are approximated in a similar fashion. Druskin and Knizhnerman (1988) used a spectral Lanczos decomposition method to obtain an arbitrary number of frequency-domain solutions at a substantially lower numerical cost. Moreover, they pioneered the use of (polynomial) Krylov methods to evaluate transients directly in the time domain (Druskin and Knizhnerman 1994; Druskin et al. 1999) and subsequently extended their research towards rational Krylov methods (Knizhnerman et al. 2009; Druskin et al. 2009; Druskin et al. 2010; Druskin and Zaslavsky 2011; Druskin and Simoncini 2011; Zaslavsky et al. 2011; Druskin et al. 2014). Recently, Börner et al. (2008) combined the shift-and-invert Krylov method, a particularly simple rational Krylov method, to evaluate the matrix resolvent function in the frequency domain, obtaining the time-domain solution via subsequent fast Hankel transform.

An important issue arising in practice is the treatment of the air half-space in the presence of topography. The effect of the air layer on the electromagnetic fields in the subsurface can be accounted for by imposing a suitable boundary condition on the air-earth interface. In general, this boundary condition is nonlocal, meaning that it couple all degrees of freedom associated with the air-earth-interface, leading to dense submatrices in the finite-element discretization. In the special case of a flat earth, Fourier-techniques can be employed to obtain an explicit representation of this dense submatrix (Oristaglio and Hohmann 1984; Goldman et al. 1986; Goldman et al. 1989; Wang and Hohmann 1993) consisting of a convolution type integral, which has to be assembled and incorporated into the discretized curl-curl operator. However, inclusion of the nonlocal boundary condition reduces the overall efficiency of the numerical method and complicates the implementation. A significant advantage of rational Krylov methods over explicit time-stepping or polynomial Krylov methods is the independence of their convergence of mesh size and conductivity structure. This permits inclusion of the air half-space in the computational domain, avoiding extra modeling effort for the nonlocal boundary condition. Instead, the details of the surface topography are reflected in the finite element mesh and the element-wise constant conductivity distribution.

In this paper, which is an extension of Börner et al. (2008) to the time domain as well as higher-order rational Krylov approximations, we demonstrate how optimal *pole parameters* which determine a rational Krylov method can be obtained *a priori* using a surrogate optimization technique. The resulting poles are problem and mesh independent in the sense that they do not change with discretization features such as mesh size, finite element order or spectral interval of the system matrices, nor do they depend on the complexity of the conductivity structure. This property can be exploited to model conductivity structures with large coefficient jumps, which appear naturally when topography has to be included in the geophysical model. Moreover, our approach produces a cyclic pole sequence consisting of a small number of distinct poles selected to guarantee an a priori determined level of accuracy in the transient within a known number of iterations. When combined with direct methods for the solution of the discrete linear systems, this leads to considerable computational savings, since the number of matrix factorizations coincides with the number of distinct poles employed (here between one and four). In particular, the computational work for the factorizations can be amortized over all rational Krylov iterations. An additional benefit of using cyclically repeated poles is that the linear systems associated with each pole can be solved concurrently in a parallel computing environment. In this case a larger number of cyclically repeated poles may be chosen to match the number of available processing units.

The remainder of this paper is organized as follows: We first recall in Section 2 the governing partial differential equations (PDEs) of geoelectromagnetic induction in the time and frequency domains and relate these via the Fourier transform. This is followed by a description of the spatial discretization using Nédélec finite elements on a tetrahedral mesh, specifying the discrete solutions in the time and frequency domains. We reformulate the problem in terms of matrix functions. In Section 3 we derive a rational Krylov method, also known as the rational Arnoldi method, for the evaluation of the action of a matrix function on a given vector and show how this can be applied to solve the discrete problem in the time and frequency domains. We show how optimal poles can be chosen for the rational Arnoldi method for which the approximation converges uniformly with respect to both spatial mesh size and conductivity structure. In Section 4 we give an algorithmic summary of our method and conclude in Section 5 with two numerical examples. As a first problem, we consider a simple model of a layered half-space to demonstrate that our approach yields accurate results. We compare the results obtained by our method to results obtained by inverse Fourier transform of large-scale frequency-domain solutions. The choice of this simple model ensures that our results can be compared to an analytical solution. As a second numerical example, we show the performance of our method for a homogeneous half-space with topography.

2 MATHEMATICAL MODEL AND DISCRETIZATION

2.1 Governing Equations

We begin by recalling the governing equations of electromagnetic induction. Neglecting displacement currents and eliminating the magnetic field, the time-dependent Maxwell's equations for the electric field intensity $\boldsymbol{e} = \boldsymbol{e}(\boldsymbol{x}, t)$ read

$$\sigma \partial_t \boldsymbol{e} + \nabla \times (\mu^{-1} \nabla \times \boldsymbol{e}) = -\partial_t \boldsymbol{j}^e, \qquad t \in \mathbb{R}. \tag{1}$$

The spatial coordinate $\boldsymbol{x}$ is assumed to vary in a computational domain $\Omega \subset \mathbb{R}^3$ containing the air-Earth interface. The magnetic permeability $\mu = \mu_0 = 4\pi \cdot 10^{-7}$ Vs/Am is that of free space and the electric conductivity $\sigma = \sigma(\boldsymbol{x})$ is a given function defined on

Ω. Along the boundary $\partial\Omega$ of Ω we impose the perfect conductor boundary condition

$$\boldsymbol{n} \times \boldsymbol{e} = \boldsymbol{0}, \tag{2}$$

and we make the implicit assumption that the boundary has been placed at sufficient distance from sources that the effects of the boundary conditions are negligible compared to discretization errors.

2.2 Source Terms

We consider a source density $\boldsymbol{j}^e$ resulting from a stationary transmitter with a driving current that is shut off at time $t = 0$, giving

$$\boldsymbol{j}^e(\boldsymbol{x}, t) = \boldsymbol{q}(\boldsymbol{x})H(-t), \tag{3}$$

in which H denotes the Heaviside unit step function and the vector field $\boldsymbol{q}$ denotes the spatial current pattern. Specifically, we consider a transmitter consisting of a small horizontal square wire-loop carrying a stationary current, thus generating a good approximation of a vertical magnetic dipole. In particular, we note that the resulting current density is divergence-free, i.e.,

$$\nabla\cdot\, \boldsymbol{q} = 0. \tag{4}$$

2.3 Time-Domain Formulation

Denoting by $\delta(t) = \partial_t H(t)$ the Dirac delta distribution concentrated at the origin $t = 0$, the combination of (1), (2) and (3) results in the boundary value problem

$$\sigma\partial_t \boldsymbol{e} + \nabla\times(\mu^{-1}\,\nabla\times \boldsymbol{e}) = \boldsymbol{q}(\boldsymbol{x})\delta(t) \quad \text{on } \Omega\times\mathbb{R}, \tag{5a}$$

$$\boldsymbol{n} \times \boldsymbol{e} = \boldsymbol{0} \quad \text{along } \partial\Omega \tag{5b}$$

for the electric field intensity $\boldsymbol{e}$ as a function of time and space on the entire time axis. For time-domain simulations it is more convenient to formulate (5) as the initial-boundary value problem

$$\sigma\partial_t \boldsymbol{e} + \nabla\times(\mu^{-1}\,\nabla\times \boldsymbol{e}) = \boldsymbol{0} \quad \text{on } \Omega\times(0,\infty), \tag{6a}$$

$$\sigma\,\boldsymbol{e}|_{t=0} = \boldsymbol{q} \quad \text{on } \Omega, \tag{6b}$$

$$\boldsymbol{n} \times \boldsymbol{e} = \boldsymbol{0} \quad \text{on } \partial\Omega\times(0,\infty). \tag{6c}$$

2.4 Frequency-Domain Formulation

To formulate the same problem in the frequency domain, we apply the Fourier transform in time, denoted by the operator $\mathscr{F}$, to both sides of (1), and introduce the transformed electric field

$$\boldsymbol{E}(\boldsymbol{x},\omega) := (\mathscr{F}\boldsymbol{e})(\omega) = \int_{-\infty}^{\infty} \boldsymbol{e}(\boldsymbol{x},t)\,\mathrm{e}^{-i\omega t}\,\mathrm{d}t, \qquad \omega\in\mathbb{R},$$

where the *angular frequency* ω has units rad/s. Observing the correspondence $(\mathscr{F}H)(\omega) = \pi\delta(\omega) + \frac{1}{i\omega}$, where δ denotes the Dirac delta distribution concentrated at zero, as well as the scaling and derivative laws for the Fourier transform, we obtain the frequency-domain equation

$$\nabla\times(\mu^{-1}\,\nabla\times \boldsymbol{E}) + i\omega\sigma\boldsymbol{E} = -i\omega\boldsymbol{q}\left(\pi\delta(\omega) - \frac{1}{i\omega}\right), \qquad \omega\in\mathbb{R}. \tag{7}$$

To simplify the problem, we introduce the impulse response electric field $\boldsymbol{e}_i = \boldsymbol{e}_i(\boldsymbol{x},t)$ as the solution of (1) with impulsive source current $\boldsymbol{j}_i^e(\boldsymbol{x},t) = \boldsymbol{q}(\boldsymbol{x})\delta(t)$. In view of the relation $(\mathscr{F}\delta)(\omega)\equiv 1$, its Fourier transform $\boldsymbol{E}_i = \boldsymbol{E}_i(\boldsymbol{x},\omega)$ satisfies

$$\nabla\times(\mu^{-1}\,\nabla\times \boldsymbol{E}_i) + i\omega\sigma\boldsymbol{E}_i = -i\omega\boldsymbol{q}. \tag{8}$$

Since both $\boldsymbol{E}$ and $\boldsymbol{E}_i$ in equations (7) and (8) satisfy the same homogeneous boundary condition (2) and the same PDE with right-hand sides which are both scalar multiples of $\boldsymbol{q}$, we conclude that

$$\boldsymbol{E}(\omega) = \left(\pi\delta(\omega) - \frac{1}{i\omega}\right)\boldsymbol{E}_i(\omega). \tag{9}$$

Transforming back to the time domain results in the transient solution

$$\begin{aligned}\boldsymbol{e}(\boldsymbol{x},t) &= \frac{1}{2\pi}\int_{-\infty}^{\infty} \boldsymbol{E}(\boldsymbol{x},\omega)\,e^{i\omega t}\,\mathrm{d}\omega\\ &= \frac{1}{2\pi}\int_{-\infty}^{\infty}\left(\pi\delta(\omega) - \frac{1}{i\omega}\right)\boldsymbol{E}_i(\omega)\,e^{i\omega t}\,\mathrm{d}\omega\\ &= \frac{1}{2}\boldsymbol{E}_i(0) - \frac{1}{2\pi}\int_{-\infty}^{\infty}\frac{\boldsymbol{E}_i(\omega)}{i\omega}\,e^{i\omega t}\,\mathrm{d}\omega, \qquad t\in\mathbb{R},\end{aligned} \tag{10}$$

where the DC component $\boldsymbol{E}_i(0)$ vanishes since the source field $\boldsymbol{q}$ is divergence-free.

2.5 Finite Element Discretization

Our numerical approximation for both the time- and frequency-domain formulations is based on a finite element discretization in space using first-kind Nédélec spaces on unstructured tetrahedral meshes. A theoretical background on Nédélec elements can be found in Monk (2003); their implementation is described in Gopalakrishnan et al. (2005) and Kirby (2014).

2.5.1 Variational Formulation

The standard variational formulation for Maxwell's equations seeks the electric field in the Sobolev space

$$\boldsymbol{H}(\mathrm{curl};\Omega) = \{\boldsymbol{u}\in L^2(\Omega)^3 : \nabla\times\boldsymbol{u}\in L^2(\Omega)^3\}.$$

Here $L^2(\Omega)^3$ denotes the space of square integrable 3-D vector fields defined on Ω. Since we impose the homogeneous boundary condition (2) along the entire boundary $\partial\Omega$, we restrict these fields further to the subspace

$$\mathscr{V} := \{\boldsymbol{u}\in\boldsymbol{H}(\mathrm{curl};\Omega) : \boldsymbol{n}\times\boldsymbol{u} = \boldsymbol{0} \text{ along } \partial\Omega\}.$$

Multiplying (6) by an arbitrary stationary vector field $\boldsymbol{\phi}\in\mathscr{V}$ and integrating by parts yields the variational problem of seeking $\boldsymbol{e} = \boldsymbol{e}(\boldsymbol{x},t)\in C([0,\infty);\mathscr{V})$ such that

$$(\sigma\partial_t\boldsymbol{e},\boldsymbol{\phi}) + (\mu^{-1}\,\nabla\times\boldsymbol{e},\nabla\times\boldsymbol{\phi}) = \boldsymbol{0}, \qquad t\in(0,\infty), \tag{11a}$$

$$(\sigma\,\boldsymbol{e}|_{t=0},\boldsymbol{\phi}) = (\boldsymbol{q},\boldsymbol{\phi}), \tag{11b}$$

for all $\boldsymbol{\phi}\in\mathscr{V}$, where $(\cdot,\cdot)$ denotes the inner product on $L^2(\Omega)^3$.

2.5.2 Discretization in Space

We employ a Galerkin discretization in space obtained by restricting the trial and test functions $\boldsymbol{e}$ and $\boldsymbol{\phi}$ in the weak form (11) to a finite-dimensional subspace $\mathscr{V}^h\subset\mathscr{V}$ consisting of first-kind Nédélec finite elements on a tetrahedral mesh $\mathscr{T}_h$. Nédélec elements are a natural approximation of electromagnetic vector fields in that they are curl-conforming, i.e., they mimic the tangential continuity properties of the fields under approximation, permitting jumps in the normal field components whenever the conductivity is discontinuous across an interface. On each tetrahedron $K\in\mathscr{T}_h$ the functions in $\mathscr{V}^h$ consist of vector polynomials $\boldsymbol{v}\in\mathscr{P}_{k-1}^3\oplus\mathscr{S}_k$,

where $\mathscr{P}_k$ denotes the space of polynomials in three variables of complete degree $k \in \mathbb{N}_0$ and

$$\mathscr{S}_k = \{\boldsymbol{v} \in \widetilde{\mathscr{P}}_k^3 : \boldsymbol{v} \cdot \boldsymbol{x} = \boldsymbol{0}\}$$

with $\widetilde{\mathscr{P}}_k$ denoting the space of homogeneous polynomials of (exact) degree k. In our numerical experiments we have used Nédélec elements of order $k = 1$ and $k = 2$, sometimes also known as *linear* and *quadratic* Nédélec elements. The discrete approximation of the solution of the variational formulation (11) is then obtained by restricting it to the subspace $\mathscr{V}^h$, i.e., by determining $\boldsymbol{e}^h \subset \mathscr{V}^h$ such that, for all test functions $\boldsymbol{\phi} \in \mathscr{V}^h$, there holds

$$(\sigma \partial_t \boldsymbol{e}^h, \boldsymbol{\phi}) + (\mu^{-1} \nabla\times \boldsymbol{e}^h, \nabla\times \boldsymbol{\phi}) = \boldsymbol{0}, \quad t > 0, \tag{12a}$$

$$(\sigma \boldsymbol{e}^h|_{t=0}, \boldsymbol{\phi}) = (\boldsymbol{q}, \boldsymbol{\phi}). \tag{12b}$$

Expanding the discrete solution $\boldsymbol{e}^h \in \mathscr{V}^h$ in a basis $\{\boldsymbol{\phi}_1, \ldots, \boldsymbol{\phi}_N\}$ of $\mathscr{V}^h$, (12) becomes the ODE initial-value problem

$$\mathbf{M}\partial_t \mathbf{u}(t) + \mathbf{C}\mathbf{u}(t) = \mathbf{0}, \quad t \in (0, \infty), \qquad \mathbf{M}\mathbf{u}(0) = \mathbf{q}, \tag{13}$$

for the vector $\mathbf{u}(t)$ containing the N coefficients of the finite element approximation $\boldsymbol{e}^h(t)$ with respect to the Nédélec basis at time $t \geq 0$. Here the mass and curl-curl matrices $\mathbf{M}$ and $\mathbf{C}$ as well as the vector $\mathbf{q}$ of initial values are given in terms of the Nédélec basis by

$$[\mathbf{M}]_{i,j} = (\sigma\boldsymbol{\phi}_j, \boldsymbol{\phi}_i), \quad [\mathbf{C}]_{i,j} = (\mu^{-1}\nabla\times\boldsymbol{\phi}_j, \nabla\times\boldsymbol{\phi}_i),$$
$$[\mathbf{q}]_i = (\boldsymbol{q}, \boldsymbol{\phi}_i), \qquad \text{for } i, j = 1, \ldots, N.$$

For the frequency-domain formulation we may employ the same spatial discretization, in terms of which (8) becomes the linear system of equations

$$(\mathbf{C} + i\omega\mathbf{M})\mathbf{u}(\omega) = -i\omega\mathbf{q} \tag{14}$$

for the coefficient vector $\mathbf{u}(\omega)$ of the impulse-response solution at frequency ω with respect to the Nédélec basis.

2.5.3 Representation as Matrix Functions

Once the TEM problem has been discretized in space, TEM forward modelling in either the time- or frequency domain formulation consists in evaluating the finite element representation of the solution of (13) for the desired values of t or solving (14) for sufficiently many frequencies to construct the transient solution via fast Hankel transform.

The explicit solution of the semi-discretized time-domain problem (13) is given in terms of the matrix exponential function

$$\mathbf{u}(t) = \exp(-t\mathbf{M}^{-1}\mathbf{C})\mathbf{M}^{-1}\mathbf{q} = f^t(\mathbf{A})\mathbf{b}, \tag{15}$$

with

$$f^t(z) = \exp(-tz), \quad \mathbf{A} = \mathbf{M}^{-1}\mathbf{C}, \quad \mathbf{b} = \mathbf{M}^{-1}\mathbf{q}.$$

Similarly, the finite element discretization (14) of the frequency-domain problem (8) has the solution

$$\mathbf{u}(\omega) = -i\omega(\mathbf{C} + i\omega\mathbf{M})^{-1}\mathbf{q} = -i\omega(\mathbf{A} + i\omega\mathbf{I})^{-1}\mathbf{b}, \tag{16}$$

so that

$$\mathbf{u}(\omega) = g^\omega(\mathbf{A})\mathbf{b} \quad \text{with} \quad g^\omega(z) = \frac{i\omega}{z + i\omega}.$$

Applying the inverse Fourier transform (10) back to the time domain to the discrete frequency-domain solution vector $\mathbf{u}(\omega)$ yields

$$(\mathscr{F}^{-1}\mathbf{u})(t) = \frac{1}{2\pi}\int_{-\infty}^{\infty}(\mathbf{A} + i\omega\mathbf{I})^{-1}\mathbf{b}e^{i\omega t}\,\mathrm{d}\omega. \tag{17}$$

To show that the transformed discrete frequency-domain solution agrees with that of the time domain, we express the latter using contour integration. Recall that, as an entire function, the function f^t in (15) may be represented as the Cauchy integral

$$f^t(z) = \frac{1}{2\pi i}\int_\Gamma \frac{f^t(\zeta)}{\zeta - z}\,\mathrm{d}\zeta, \tag{18}$$

where Γ is a contour surrounding the point z in the complex plane. The same contour integral may be used to evaluate $f^t(\mathbf{A})$ provided the contour Γ contains all eigenvalues of $\mathbf{A}$ in its interior. Since

$$\mathbf{M}^{1/2}\mathbf{A}\mathbf{M}^{-1/2} = \mathbf{M}^{-1/2}\mathbf{C}\mathbf{M}^{-1/2},$$

we see that $\mathbf{A}$ is similar to the matrix on the right-hand side, which is symmetric and, since $\mathbf{M}$ is symmetric positive definite and $\mathbf{C}$ symmetric positive semidefinite, is also symmetric positive semidefinite. The eigenvalues of $\mathbf{A}$ therefore lie on the nonnegative real axis. The zero eigenvalues of $\mathbf{C}$ are associated with discrete gradient fields. These are not present in the given solution due to the fact that the field $\boldsymbol{q}$ is divergence-free. We may therefore ignore the zero eigenvalue and use the imaginary axis as the integration contour in (18). Parametrizing the imaginary axis by $-i\omega$, $\omega \in (-\infty, \infty)$, we obtain

$$\begin{aligned}\mathbf{u}(t) &= f^t(\mathbf{A})\mathbf{b} = \frac{1}{2\pi i}\int_\Gamma (\zeta\mathbf{I} - \mathbf{A})^{-1} f^t(\zeta)\,\mathrm{d}\zeta\ \mathbf{b} \\ &= \frac{1}{2\pi}\int_{-\infty}^{\infty}(\mathbf{A} + i\omega\mathbf{I})^{-1}e^{i\omega t}\,\mathrm{d}\omega\ \mathbf{b},\end{aligned}$$

which coincides with (17).

3 RATIONAL ARNOLDI APPROXIMATION

We have seen in the previous section that the the solution vector $\mathbf{u}$ containing the finite element coefficients of the solution of the TEM forward modeling problem can be expressed as a matrix function applied to a vector: in the time-domain formulation this is the matrix exponential function (15) while in the frequency domain this is the (matrix) resolvent function (16). When the matrices involved are large and sparse, as is the case with matrices arising from finite element discretization of Maxwell's equations, Krylov subspace methods can be applied to construct efficient approximations of such matrix function evaluations. In this section we briefly recall a popular rational Krylov method, also known as the rational Arnoldi method, for approximating the action $f(\mathbf{A})\mathbf{b}$ of a generic matrix function f. Our variant of this method uses an orthogonalization procedure in the $\mathbf{M}$-inner product defined as $\langle \mathbf{x}, \mathbf{y}\rangle_\mathbf{M} := \mathbf{y}^H\mathbf{M}\mathbf{x}$ with induced norm $\|\mathbf{x}\|_\mathbf{M} := \sqrt{\langle \mathbf{x}, \mathbf{x}\rangle_\mathbf{M}}$. Here $\mathbf{y}^H$ denotes the complex conjugate transpose of $\mathbf{y}$. For the problem under consideration the symmetric positive definite matrix $\mathbf{M}$ defining the inner product will be the finite element mass matrix.

We use the rational Krylov orthogonalization algorithm of Ruhe (1994) to construct a sequence of orthonormal vectors $\{\mathbf{v}_j\}_{j\geq 1}$. Starting with the vector $\mathbf{v}_1 = \mathbf{b}/\|\mathbf{b}\|_\mathbf{M}$, we determine in each step a vector $\mathbf{v}_{j+1}$ which is $\mathbf{M}$-orthogonal to the previously generated vectors $\mathbf{v}_1, \mathbf{v}_2, \ldots, \mathbf{v}_j$. This leads to the recursion

$$\mathbf{v}_{j+1}h_{j+1,j} = (\mathbf{A} - \xi_j\mathbf{I})^{-1}\mathbf{v}_j - \sum_{i=1}^{j}\mathbf{v}_i h_{i,j}, \quad j = 1, 2, \ldots, m, \tag{19}$$

where the coefficients are defined as $h_{i,j} = \langle (\mathbf{A} - \xi_j\mathbf{I})^{-1}\mathbf{v}_j, \mathbf{v}_i\rangle_\mathbf{M}$,

and $h_{j+1,j} > 0$ is chosen such that $\|\mathbf{v}_{j+1}\|_{\mathbf{M}} = 1$. The numbers $\{\xi_j\}_{j=1}^m$ are parameters known as *poles* which define the rational Krylov method and will be discussed below. It is convenient to collect the computed basis vectors in a matrix $\mathbf{V}_{m+1} = [\mathbf{v}_1, \mathbf{v}_2, \ldots, \mathbf{v}_{m+1}] \in \mathbb{C}^{N\times(m+1)}$. Note that by construction we have $\mathbf{V}_{m+1}^H \mathbf{M} \mathbf{V}_{m+1} = \mathbf{I}_{m+1}$, where $\mathbf{I}_{m+1} \in \mathbb{R}^{(m+1)\times(m+1)}$ denotes the identity matrix. We can now define the *rational Arnoldi approximation for* $f(\mathbf{A})\mathbf{b}$ *of order* m as

$$\mathbf{f}_m := \|\mathbf{b}\|_{\mathbf{M}} \mathbf{V}_{m+1} f(\mathbf{A}_{m+1}) \mathbf{e}_1, \quad \mathbf{A}_{m+1} := \mathbf{V}_{m+1}^H \mathbf{M} \mathbf{A} \mathbf{V}_{m+1}, \tag{20}$$

where $\mathbf{e}_1 = [1, 0, \ldots, 0]^T \in \mathbb{R}^{m+1}$. The matrix $\mathbf{A}_{m+1}$, also known as the *matrix Rayleigh quotient*, is the $\mathbf{M}$-orthogonal projection of $\mathbf{A}$ with respect to $\mathbf{V}_{m+1}$. It is of size $(m+1)\times(m+1)$, hence, if $m \ll N$, computing $f(\mathbf{A}_{m+1})$ becomes feasible, whereas that of $f(\mathbf{A})$ is not. As an example, in our numerical experiments in Section 5 we consider values of at most $m = 72$, whereas N, the number of degrees of freedom in the finite element model, can easily range in the hundreds of thousands. The set of eigenvalues $\Lambda(\mathbf{A}_{m+1})$ of this projected matrix are known as *rational Ritz values* (see, e.g., Beckermann et al. 2010) and, as we shall see below, play an important role in rational Arnoldi approximations.

We next recall two results from the theory of rational Krylov subspaces which are the key to analyzing the accuracy of the associated approximations. In essence, they show that the error of the rational Arnoldi approximation (20) to $f(\mathbf{A})\mathbf{b}$ can be bounded in terms of the error of (scalar) interpolation of the function f on the set of rational Ritz values by particularly simple rational functions. The first result characterizes the rational Arnoldi approximation $\mathbf{f}_m$ in terms of a rational function r_m interpolating the function f. Several variants of this result have appeared in the literature, both for polynomial (Ericsson 1990; Saad 1992) and rational Krylov spaces (Beckermann and Reichel 2009 or Güttel 2010, Theorem 5.8). Here and in the following, $\mathscr{P}_m$ denotes the linear space of all polynomials of degree at most m, and $\mathscr{P}_m/q_m$ is the linear space of rational functions of type (m, m) with a prescribed denominator polynomial q_m.

Theorem 3.1. The rational Arnoldi approximation $\mathbf{f}_m$ of $f(\mathbf{A})\mathbf{b}$ defined in (20) satisfies

$$\mathbf{f}_m = r_m(\mathbf{A})\mathbf{b},$$

where $r_m \in \mathscr{P}_m/q_m$ interpolates f in the Hermite sense (i.e., counting multiplicities) at the rational Ritz values $\Lambda(\mathbf{A}_{m+1})$, and $q_m(z) = (z-\xi_1)(z-\xi_2)\cdots(z-\xi_m)$.

It follows from Theorem 3.1 that the rational Arnoldi approximation $\mathbf{f}_m$ is exact if f is itself a rational function in $\mathscr{P}_m/q_m$, i.e., a rational function of type (m, m) with prescribed denominator q_m. This exactness implies that $\mathbf{f}_m$ satisfies a so-called *near-optimality property* in the $\mathbf{M}$-norm. By near-optimality is meant that the rational function r_m underlying the rational Arnoldi approximation $\mathbf{f}_m$ is close to the best uniform rational approximant to f over the spectral interval of the matrix $\mathbf{A}$. (The spectral interval is the smallest real interval containing the eigenvalues of $\mathbf{A}$). The poles of this rational function are precisely the *pole parameters* $\xi_1, \xi_2, \ldots, \xi_m$ used in the recursion (19), and the following theorem is key to our pole selection approach. Similar results regarding near-optimality in the 2-norm have been given in (Ericsson 1990; Saad 1992; Beckermann and Reichel 2009; Güttel 2010).

Theorem 3.2. The rational Arnoldi approximation $\mathbf{f}_m$ to $f(\mathbf{A})\mathbf{b}$ defined in (20) satisfies

$$\|f(\mathbf{A})\mathbf{b} - \mathbf{f}_m\|_{\mathbf{M}} \le 2\|\mathbf{b}\|_{\mathbf{M}} \min_{r_m \in \mathscr{P}_m/q_m} \max_{z\in[\alpha,\beta]} |f(z) - r_m(z)|, \tag{21}$$

where $[\alpha, \beta]$ is an interval containing the eigenvalues of $\mathbf{A} = \mathbf{M}^{-1}\mathbf{C}$.

Proof: A straightforward calculation using the triangle inequality for vector norms and the fact that, for any rational function $r_m \in \mathscr{P}_m/q_m$, there holds $r_m(\mathbf{A})\mathbf{b} = \|\mathbf{b}\|_{\mathbf{M}} \mathbf{V}_{m+1} r_m(\mathbf{A}_{m+1})\mathbf{e}_1$ by Theorem 3.1, shows

$$\begin{aligned}
& \|f(\mathbf{A})\mathbf{b} - \mathbf{f}_m\|_{\mathbf{M}} \\
= \; & \|f(\mathbf{A})\mathbf{b} - r_m(\mathbf{A})\mathbf{b} + r_m(\mathbf{A})\mathbf{b} - \mathbf{f}_m\|_{\mathbf{M}} \\
\le \; & \|f(\mathbf{A})\mathbf{b} - r_m(\mathbf{A})\mathbf{b}\|_{\mathbf{M}} \\
& \quad + \|\mathbf{b}\|_{\mathbf{M}} \cdot \|\mathbf{V}_{m+1} r_m(\mathbf{A}_{m+1})\mathbf{e}_1 - \mathbf{V}_{m+1} f(\mathbf{A}_{m+1})\mathbf{e}_1\|_{\mathbf{M}}.
\end{aligned}$$

We now bound from above each of the two terms in this sum. For the first term we use the facts that $g(\mathbf{A}) = \mathbf{M}^{-1/2} g(\mathbf{M}^{1/2}\mathbf{A}\mathbf{M}^{-1/2})\mathbf{M}^{1/2}$ for any function g such that $g(\mathbf{A})$ is a well-defined matrix function, the matrix $\mathbf{M}^{1/2}\mathbf{A}\mathbf{M}^{-1/2}$ is Hermitian and similar to $\mathbf{A}$, and $\|\mathbf{M}^{-1/2}\mathbf{x}\|_{\mathbf{M}} = \|\mathbf{x}\|_2$. We obtain

$$\begin{aligned}
& \|(f - r_m)(\mathbf{A})\mathbf{b}\|_{\mathbf{M}} \\
= \; & \|\mathbf{M}^{-1/2}(f - r_m)(\mathbf{M}^{1/2}\mathbf{A}\mathbf{M}^{-1/2})\mathbf{M}^{1/2}\mathbf{b}\|_{\mathbf{M}} \\
= \; & \|(f - r_m)(\mathbf{M}^{1/2}\mathbf{A}\mathbf{M}^{-1/2})\mathbf{M}^{1/2}\mathbf{b}\|_2 \\
\le \; & \|(f - r_m)(\mathbf{M}^{1/2}\mathbf{A}\mathbf{M}^{-1/2})\|_2 \|\mathbf{M}^{1/2}\mathbf{b}\|_2 \\
= \; & \|\mathbf{b}\|_{\mathbf{M}} \max_{\lambda\in\Lambda(\mathbf{A})} |f(\lambda) - r_m(\lambda)|.
\end{aligned}$$

For the second term we have

$$\begin{aligned}
\|\mathbf{V}_{m+1}(r_m - f)(\mathbf{A}_{m+1})\mathbf{e}_1\|_{\mathbf{M}} &= \|(r_m - f)(\mathbf{A}_{m+1})\mathbf{e}_1\|_2 \\
&\le \|(r_m - f)(\mathbf{A}_{m+1})\|_2 \\
&\le \max_{\lambda\in\Lambda(\mathbf{A}_{m+1})} |r_m(\lambda) - f(\lambda)|,
\end{aligned}$$

where we have used the fact $\|\mathbf{V}_{m+1}\mathbf{x}\|_{\mathbf{M}} = \|\mathbf{x}\|_2$. Adding both inequalities and noting that $\Lambda(\mathbf{A}_{m+1})$ is contained in the spectral interval of $\mathbf{A}$, and taking the maximum over all admissible rational functions $r_m \in \mathscr{P}_m/q_m$ completes the proof. □

The stated results now enable us to propose our new strategy for selecting the poles $\xi_1, \xi_2, \ldots, \xi_m$ (the zeros of q_m) for the TEM forward modeling problem.

3.1 Error Estimation Using a Surrogate Problem

The near-optimality property stated in Theorem 3.2 means that the optimization of parameters for the rational Arnoldi approximation $\mathbf{f}_m$ defined in (20) essentially reduces to the problem of finding a denominator polynomial q_m such that the right-hand side of the error bound (21) is minimized. Recall that the zeros $\xi_1, \ldots, \xi_m$ of q_m correspond to the poles used in the recursion (19) for constructing a basis $\mathbf{V}_{m+1}$ of the rational Krylov space. Given such a polynomial q_m and an interval $[\alpha, \beta]$, the min-max expression on the right of (21) could be computed by the Remez algorithm for best uniform approximation of f on $[\alpha, \beta]$ (see, e.g., Meinardus and Schumaker 1967). However, the computation of best rational approximants can suffer numerical instabilities and, in addition, our problem is complicated by the fact that we are ultimately interested in rational approximation of parameter-dependent functions $f(z) = f^t(z) = \exp(-tz)$ or $f(z) = g^\omega(z) = i\omega/(z + i\omega)$ in the time- and frequency-domain cases, respectively.

We propose an alternative approach which is tailored to our problem and computationally more robust: we will estimate the min-max expression (21) by using the rational Arnoldi method itself, applied to a diagonal matrix, the inversion of which is trivial, possessing a sufficiently large and dense spectrum on the nonnegative real axis. For ease of exposition we first consider the problem of parameter-independent approximation of f and then introduce the parameter for f^t or g^ω later.

Given the function f and a denominator polynomial q_m, our aim is to estimate the error

$$\mathrm{err}(f, q_m) := \min_{r_m \in \mathscr{P}_m/q_m} \max_{z\in[0,+\infty]} |f(z) - r_m(z)|.$$

Note that we have formally set $[\alpha, \beta] = [0, +\infty]$ because this will allow us to obtain error bounds that are independent of the spectral interval of $\mathbf{A}$ (which will lead to a rational Arnoldi method that converges independently of the spatial mesh and the conductivity structure, or in other words, exhibits robust convergence). The quantity $\max_{z\in[0,+\infty]} |f(z)-r_m(z)|$ will exist if f is bounded on $[0, +\infty]$ and r_m has no poles there. Both conditions are naturally satisfied in our situation where $f = f^t$ or $f = g^\omega$, respectively.

In order to avoid working with an unbounded interval we introduce the variable $\hat{z} \in [1, 2]$, the transformation $z = (\hat{z} - 1)^{-1} - 1$, the transformed function $\hat{f}(\hat{z}) = f(z)$, and the transformed denominator $\hat{q}_m(\hat{z}) = (\hat{z} - \hat{\xi}_1)\cdots(\hat{z} - \hat{\xi}_m)$, where each $\hat{\xi}_j = (\xi_j + 1)^{-1} + 1$. Instead of the above expression for the error we now consider

$$\mathrm{err}(f, q_m) = \min_{\hat{r}_m \in \mathscr{P}_m/\hat{q}_m} \max_{\hat{z}\in[1,2]} |\hat{f}(\hat{z}) - \hat{r}_m(\hat{z})|.$$

We then use the rational Arnoldi method for approximating $\hat{f}(\widehat{\mathbf{A}})\widehat{\mathbf{b}}$ in the Euclidian inner product with a diagonal surrogate matrix $\widehat{\mathbf{A}}$ having sufficiently dense eigenvalues in $[1, 2]$, and the vector $\widehat{\mathbf{b}} = [1, \ldots, 1]^T$. Let the associated rational Arnoldi approximation be denoted as $\widehat{\mathbf{f}}_m = \hat{r}_m(\widehat{\mathbf{A}})\widehat{\mathbf{b}}$. Then by the diagonal form of $\widehat{\mathbf{A}}$ and the definition of $\widehat{\mathbf{b}}$ we have

$$\begin{aligned} \|\hat{f}(\widehat{\mathbf{A}})\widehat{\mathbf{b}} - \widehat{\mathbf{f}}_m\|_\infty &= \max_{\hat{\lambda}\in\Lambda(\widehat{\mathbf{A}})} |\hat{f}(\hat{\lambda}) - \hat{r}_m(\hat{\lambda})| \\ &\le \max_{\hat{z}\in[1,2]} |\hat{f}(\hat{z}) - \hat{r}_m(\hat{z})|, \end{aligned} \tag{22}$$

where the expression on the left-hand side is easy to compute as $\hat{f}(\widehat{\mathbf{A}})\widehat{\mathbf{b}}$ is explicitly known (a function of a diagonal matrix is the diagonal matrix of the function values). Note that building a rational Krylov basis with $\widehat{\mathbf{A}}$ is computationally inexpensive as we only need to solve linear systems with diagonal matrices.

As becomes clear from (22) we can only compute an approximate upper bound for $\mathrm{err}(f, q_m)$ with the described procedure. However, the inequality in (22) can be expected to be sufficiently sharp if $\Lambda(\widehat{\mathbf{A}})$ is a sufficiently dense discretization of $[1, 2]$, so that "spectral adaptation" in the rational Arnoldi method does not yet occur (which means that the method behaves as if the spectrum of $\widehat{\mathbf{A}}$ were a continuum). A detailed analysis of spectral adaptation in the rational Arnoldi method is given in Beckermann et al. (2010) and Beckermann and Güttel (2012), where it is shown that the region of "deflated eigenvalues" depends on the ratio $m/\widehat{N}$, that is, the number of rational Arnoldi iterations m compared to the size $\widehat{N}$ of the surrogate matrix $\widehat{\mathbf{A}}$. For all numerical results reported below, specifically in Table 1, we have used $m \le 72$ and found that, with a diagonal matrix $\widehat{\mathbf{A}}$ having $\widehat{N} = 3000$ equidistant eigenvalues in the interval $[1, 2]$, no noticeable spectral adaptation occurred. Further increase of $\widehat{N}$ did not change the results in any digit reported in Table 1.

We remark that more elaborate strategies for choosing $\widehat{N}$ and the eigenvalues of the surrogate $\widehat{\mathbf{A}}$ could be motivated by the interpolation characterization in Theorem 3.1. For example, one could start with a small number of $\widehat{N}_1 = 2m$ equispaced eigenvalues and then refine the spectrum to $\widehat{N}_2, \widehat{N}_3, \ldots$ eigenvalues by adding geometric means of rational Ritz values. We have not implemented such a strategy here as the pole optimization is a one-time calculation requiring negligible computing time compared to the solution of the forward modeling problem.

3.2 Pole Optimization

Now that $\mathrm{err}(f, q_m)$ can be estimated efficiently for a given q_m and any function $f = f^t$ (all rational Arnoldi approximants $\widehat{\mathbf{f}}_m^t$ for $f^t(\widehat{\mathbf{A}})\widehat{\mathbf{b}}$ can be extracted from the same rational Krylov space), it remains to find a fixed "optimal" q_m which minimizes $\mathrm{err}(f^t, q_m)$ uniformly for all parameters $t \in [t_{\min}, t_{\max}]$. This constitutes a constrained nonlinear optimization problem:

(P0) Find $q_m(z) = \prod_{j=1}^m (z - \xi_j)$ such that

$$\max_{t\in[t_{\min},t_{\max}]} \mathrm{err}(f^t, q_m) \approx \max_{t\in[t_{\min},t_{\max}]} \|\hat{f}^t(\widehat{\mathbf{A}})\widehat{\mathbf{b}} - \widehat{\mathbf{f}}_m^t\|_\infty$$

is minimal, with the constraint that the poles ξ_j be negative.

To enable the efficient solution of this problem we have applied two further constraints. First, we assume that m is divisible by an integer $\ell < m$ and q_m is factored in the form

$$q_m(z) = \prod_{j=1}^{\ell} (z - \xi_j)^{m/\ell}.$$

This reduces the problem of finding m parameters to that of finding merely ℓ parameters. Note, however, that this constraint on the factorization of q_m leads to the somewhat counter-intuitive effect that, for m constant, the error $\mathrm{err}(f^t, q_m)$ may slightly increase as the number of distinct parameters ℓ increases (see, for example, Table 1). The poles $\xi_1, \ldots, \xi_\ell$ correspond to shifts in linear system solves in (19), so reusing the shifts for m/ℓ rational Arnoldi iterations is convenient when direct solvers are employed (see also the discussion in Section 4).

Second, for $f^t(z) = \exp(-tz)$ we can restrict the set of admissible poles further by considering the best uniform rational approximant r_m of the form $p_m(z)/(z - \xi)^m$, $p_m \in \mathscr{P}_m$, minimizing $\max_{z\in[0,\infty]} |\exp(-z) - r_m(z)|$, i.e., the rational approximant having all poles concentrated at $\xi < 0$. By scaling z to tz we find that the best uniform rational approximant r_m of type (m, m) with concentrated negative poles that minimizes $\max_{z\in[0,\infty]} |\exp(-tz) - r_m(z)|$ must be of the form $p_m(z)/(tz - \xi)^m$, $p_m \in \mathscr{P}_m$, i.e., all poles are concentrated at $\xi/t < 0$. It is therefore reasonable to restrict the poles $\xi_1, \ldots, \xi_\ell$ for uniform approximation of $f^t(z) = \exp(-tz)$ with $t \in [t_{\min}, t_{\max}]$ to the interval $[\xi_{\min}, \xi_{\max}]$, where $\xi_{\min} < 0$ is the optimal concentrated pole of the rational approximant $p_m(z)/(tz - \xi_{\min})^m$ for $\exp(-t_{\min} z)$, and $\xi_{\max} = \xi_{\min} t_{\min}/t_{\max}$.

Summarizing, we have arrived at the following optimization problem:

(P1) Find $q_m(z) = \prod_{j=1}^{\ell} (z - \xi_j)^{m/\ell}$ such that

$$\max_{t\in[t_{\min},t_{\max}]} \mathrm{err}(f^t, q_m) \approx \max_{t\in[t_{\min},t_{\max}]} \|\hat{f}^t(\widehat{\mathbf{A}})\widehat{\mathbf{b}} - \widehat{\mathbf{f}}_m^t\|_\infty$$

is minimal, with the constraint that all $\xi_j \in [\xi_{\min}, \xi_{\max}]$.

We have used MATLAB to solve this minimization problem for the time interval $[t_{\min}, t_{\max}] = [10^{-6}, 10^{-3}]$, with $m = 12, 24, \ldots, 72$ and $\ell = 1, 2, 3, 4$. As this problem seems to have many local minima, we determined the parameters $\xi_1, \ldots, \xi_\ell$ by first performing a global search on a coarse discretization of $[\xi_{\min}, \xi_{\max}]$ with 100 logarithmically equispaced points, and then refining the result using MATLAB's `fmincon` routine. The surrogate problem was of size $\widehat{N} = 3000$. The results are reported in Table 1.

This table can be used in the following way: if no parallel solution of linear systems is desired, Table 1 reveals that it is most efficient to use two cyclically repeated poles. To determine the optimal poles for a time interval of, say, $[10^{-6}, 10^{-3}]$, one reads off the two poles in the first row for which the desired level of accuracy is reached. The first column of this row then gives the number of required rational Arnoldi iterations m. For example, to achieve an error level below $2 \times 7.45 \cdot 10^{-8}$ (the factor 2 comes from the error bound (21)) it is sufficient to run $m = 36$ rational Arnoldi iterations, repeating the two poles $\xi_1 = -3.32e+4$ and $\xi_2 = -3.88e+06$ cyclically 18 times . By the scaling argument given above, the table can also be used for other time intervals consisting of 3 decades. For the time interval $[10^{-5}, 10^{-2}]$, for example, the poles have to be replaced by $\xi_1/10$ and $\xi_2/10$.

[Table 1 about here.]

The poles in Table 1 have been optimized to give a *uniformly* small approximation error over a time interval. We note that it is also easily possible to optimize the poles with respect to a positive weight function $w(t)$ by minimizing $\max_{t\in[t_{\min},t_{\max}]} w(t) \cdot \mathrm{err}(f^t, q_m)$. This can be used to improve the approximation in certain parts of the time interval, such as for late times, particularly when the asymptotic behavior of the transient is known from analytic solutions (cf. Ward and Hohmann (1987)).

3.3 Relation to Existing Work and Other Pole Selection Strategies

In this section we briefly review some other pole selection strategies. For a more detailed survey we refer to Güttel 2013.

The problem of optimizing a single repeated negative pole for approximating $\exp(-t_0\mathbf{A})\mathbf{b}$ for a single time point t_0 was considered in Eshof and Hochbruck 2006. In case of a single pole the corresponding rational approximation problem can be transformed into an equivalent polynomial approximation problem, and this problem can be solved numerically using the polynomial Remez algorithm Eshof and Hochbruck 2006, a stable implementation of which is available, e.g., in the Chebfun system, see Hale and L. N. Trefethen 2014. Our problem of uniform approximation on a time interval $[t_{\min}, t_{\max}]$ can be seen as a generalization, but in the case of two or more cyclically repeated poles it does not seem to be possible to find an equivalent polynomial formulation. A result bounding the error of rational Arnoldi approximants with cyclically repeated poles in terms of the error of single pole approximants was given in Güttel 2010, p. 113–115.

A different route for computing poles which are asymptotically optimal for all $t > 0$ was followed in Druskin et al. 2009. Here the constructed negative poles are given in terms of elliptic functions and it is shown that the rational Arnoldi method with these parameters will converge *for all time parameters* $t > 0$ with a geometric rate given by

$$\limsup_{m\to\infty} \| \exp(-t\mathbf{A})\mathbf{b} - \mathbf{f}_m^t \|^{1/m} \simeq \exp\left(-\frac{\pi^2}{4\log(2/\delta)}\right), \quad (23)$$

where $\mu = \left(\frac{1-\delta}{1+\delta}\right)^2$ and $\delta = \sqrt{\frac{\lambda_{\min}}{\lambda_{\max}}}$, with $\lambda_{\max}$ and $\lambda_{\min}$ denoting the largest and smallest nonzero eigenvalue of $\mathbf{A}$, respectively. The convergence rate on the right of (23) deteriorates with a growing condition number $\lambda_{\max}/\lambda_{\min}$ of $\mathbf{A}$, hence this approach cannot be expected to give convergence independent of mesh or conductivity structure. On the other hand, the rate is independent of the length of Finally, we remark that these asymptotically optimal pole sequences consist of pairwise distinct poles, so no factorizations of shifted matrices can be reused in the rational Arnoldi method when a direct solver is employed.

3.4 Relation Between Frequency and Time Domain Approaches

We have discussed an approach for approximating the transient of the TEM solution directly in time domain. However, as mentioned in Section 1, an alternative approach is to synthesize the time-domain solution from frequency-domain solutions by computing the inverse Fourier transform (10). The latter can be approximated numerically to desired accuracy by fast Hankel transform (FHT) techniques as described in Johansen and Sørensen (1979) and refined in Christensen (1990), where also bounds on the number of frequency-domain solutions required for a sufficiently accurate transient can be found. By using rational Krylov approximation in the frequency domain a uniformly accurate solution approximation $\mathbf{u}(\omega)$ is available for all frequencies as soon as a rational Krylov space of sufficiently large dimension has been constructed (cf. Börner et al. (2008)). As a consequence, considerably fewer frequency-domain problems need to be solved than necessary to obtain an accurate transient via the FHT.

In both the time and frequency domains the rational Krylov spaces are constructed using the same matrix $\mathbf{A}$ and initial vector $\mathbf{b}$, but may differ in the pole sequence, which should be chosen in an optimal fashion for the function g^ω in the frequency domain and f^t in the time domain. We argue that the frequency domain approximation followed by FHT cannot yield a significantly better approximation than that obtained in the time domain: the FHT results in a time domain approximation which is a linear combination of vectors from the rational Krylov space built from frequency-domain solutions. One could then, using the same poles as in the frequency domain, construct a rational Krylov approximation of $f^t(\mathbf{A})\mathbf{b}$, and the near-optimality of the rational Krylov approximation (see Theorem 3.2) would select an approximation which is at least as good as the FHT-transformed frequency domain approximation. Using poles in the time domain which are chosen in an optimal fashion for the function f^t would only further improve this approximation. For this reason we restrict ourselves to the time-domain case in the following sections.

4 ALGORITHMIC ASPECTS

We now summarize the method discussed in the previous sections as an algorithm, with an emphasis on some implementation issues. We only concentrate on the time domain problem. Referring to Section 2.5.3, we recall that our aim is to approximate $\mathbf{u}(t) = \exp(-t\mathbf{A})\mathbf{b}$ for multiple $t \in [t_{\min}, t_{\max}]$, where $\mathbf{A} = \mathbf{M}^{-1}\mathbf{C}$ and

Algorithm 1 Rational Arnoldi approximation of $\exp(-t\mathbf{A})\mathbf{b}$.

Inputs: Finite element matrices $\mathbf{C}$ and $\mathbf{M}$, vector $\mathbf{b}$, time points $t \in [t_{\min}, t_{\max}]$, parameters m, ℓ and poles $\xi_1, \ldots, \xi_\ell$ from Table 1.
Output: Rational Arnoldi approximations $\mathbf{f}_m^t$ for $\exp(-t\mathbf{A})\mathbf{b}$ and all time points t of interest.

```
01  FOR p = 1, ..., ℓ,
02      Compute Cholesky factorizations L_p L_p^H = C − ξ_p M.
03  END
04  Set v_1 := b/‖b‖_M.
05  FOR j = 1, ..., m,
06      Solve L_p L_p^H w = M v_j for w, where p = (j mod ℓ)+1.
07      FOR i = 1, ..., j,
08          Compute h_{i,j} := ⟨w, v_i⟩_M and w := w − v_i h_{i,j}.
09      END
10      Set v_{j+1} := w/‖w‖_M.
11  END
12  Compute A_{m+1} := V_{m+1}^H C V_{m+1}, V_{m+1} = [v_1, ..., v_{m+1}].
13  Compute f_m^t := ‖b‖_M V_{m+1} exp(−t A_{m+1}) e_1 for all t.
```

$\mathbf{b} = \mathbf{M}^{-1}\mathbf{q}$ stem from the finite element discretization described in Section 2.5.2.

The method consists of constructing an orthonormal basis $\mathbf{V}_{m+1}$ of a rational Krylov space using the orthogonalization algorithm by Ruhe (1994) in the $\mathbf{M}$-inner product.* This algorithm implements the recursion (19) and corresponds to lines 4–11 in Algorithm 1. Note that each iteration j of (19) *formally* amounts to the solution of a shifted linear system with $\mathbf{A} = \mathbf{M}^{-1}\mathbf{C}$, which generally is a dense matrix even if $\mathbf{C}$ and $\mathbf{M}$ are sparse. Practically, however, we can rewrite (19) equivalently as

$$\mathbf{v}_{j+1}h_{j+1,j} = (\mathbf{C} - \xi_j\mathbf{M})^{-1}\mathbf{M}\mathbf{v}_j - \sum_{i=1}^{j}\mathbf{v}_i h_{i,j},$$

which shows that iteration j requires the solution of a linear system with $\mathbf{C} - \xi_j\mathbf{M}$, which is sparse. With the negative poles presented in Table 1 these shifted linear systems are symmetric positive definite and can be solved either by an iterative method like multigrid or conjugate gradients Saad and Vorst 2000, or by a direct method (Cholesky factorization, see, e.g., Golub and Van Loan 1996). If Cholesky factorizations are employed, as in our numerical experiments reported in Section 5, then one can use to great advantage that our poles listed in Table 1 are repeated cyclically, i.e., the number of matrix factorizations is only as large as the number of distinct poles ℓ. The ℓ Cholesky factors can be precomputed as shown in lines 1–3 of Algorithm 1. As the factorization phase typically makes up the bulk of the computation time in a direct solver, repeated poles lead to significant savings in time-to-solution, as the computing effort for the ℓ Cholesky factorizations is amortized over all rational Krylov iterations.

Finally, we note that the matrix Rayleigh quotient $\mathbf{A}_{m+1}$ defined in (20) can be computed inexpensively via projection of $\mathbf{C}$, using again the fact that $\mathbf{A} = \mathbf{M}^{-1}\mathbf{C}$:

$$\mathbf{V}_{m+1}^H\mathbf{M}\mathbf{A}\mathbf{V}_{m+1} = \mathbf{V}_{m+1}^H\mathbf{C}\mathbf{V}_{m+1} = \mathbf{A}_{m+1}.$$

The rational Arnoldi approximations $\mathbf{f}_m^t$ defined in (20) can then be computed from the same rational Krylov space for all time points $t \in [t_{\min}, t_{\max}]$ of interest (lines 12–13 of Algorithm 1).

* A MATLAB implementation of this algorithm is available in the Rational Krylov Toolbox (Berljafa and Güttel 2014) which can be downloaded from `http://guettel.com/rktoolbox`.

5 NUMERICAL EXPERIMENTS

We present a series of numerical experiments for two model problems to illustrate the important features of the rational Arnoldi approximation in the time domain. In the first set we consider the transient response of a vertical magnetic dipole located atop a layered half-space. For this model problem there is a closed-form solution available (see Ward and Hohmann 1987), which can be used as a reference solution to analyze the contributions of the errors due to the boundary condition, the finite element discretization and the rational Arnoldi approximation. We are able to verify that the convergence of the rational Arnoldi approximation is uniform in both time and spatial discretization.

A model with terrain topography serves as a second numerical example. This illustrates one of the advantages of using rational Krylov approximations, as the computational domain can be chosen to include the air half-space without significant impact on the convergence behavior. This is in contrast to time-stepping schemes, where the minimum conductivity from inclusion of the air layer leads to excessively small time steps, and to polynomial Krylov subspace methods, for which the iteration count increases with low conductivities. We illustrate the benefit of accounting for topography by comparison with a flat-earth model.

5.1 Layered Half-Space

We first consider the model of a layered half-space. A layer with an electrical resistivity of $30\,\Omega\cdot\mathrm{m}$ and a thickness of $30\,\mathrm{m}$ is embedded in a homogeneous half-space of $100\,\Omega\cdot\mathrm{m}$ at a depth of $100\,\mathrm{m}$. A vertical magnetic dipole source is approximated by a small $10\times 10\,\mathrm{m}^2$ horizontal loop located at the Earth's surface, i.e., at $z = 0$.

The computational domain Ω consists of a cube of side length $2\,\mathrm{km}$ centered at the origin, which is also the center of the square transmitter coil. We used the mesh generator of the COMSOL Multiphysics® finite element package (Version 3.5a) to generate a tetrahedral mesh. By making the line segments which form the transmitter coil sufficiently small and specifying a sufficiently small maximal element size in the vicinity of the observation point, we obtained a mesh which is locally refined near the transmitter and receiver. Fig. 1 shows the trace of the tetrahedral mesh looking down on the surface $z = 0$, where the local refinement in the vicinity of both the dipole source and the receiver is visible. The mesh employed for the computations consists of 24,582 tetrahedra. The matrices $\mathbf{M}$ and $\mathbf{C}$ in the time- and frequency-domain discretizations (13) and (14) have dimensions $N = 27,623$ and $N = 152,078$ for the Nédélec spaces of order $k = 1$ and $k = 2$, respectively.

Fig. 2 shows the decrease of the absolute error $\|f^t(\mathbf{A})\mathbf{b} - \mathbf{f}_m^t\|_\mathbf{M}$ scaled by $\|\mathbf{b}\|_\mathbf{M}$ with respect to a sufficiently accurate reference solution of the discrete problem as the rational Arnoldi iteration progresses. Each curve within the plots corresponds to the error against the order m of the rational Krylov approximation for one discrete time between $t = 10^{-6}$s to 10^{-3}s, the location of which within the time interval is coded by the transition from red (10^{-6}s) to blue (10^{-3}s). Results are given for spatial discretization with Nédélec elements of order $k = 1$ (left column) and $k = 2$ (right column), each using $\ell = 1, 2$ and 3 cyclically repeated poles (rows one, two and three). The reference solution consisted of a rational Arnoldi approximation of high order $m = 72$ for $\ell = 2$. The choice of this particular reference solution is based on the observation that, with a value of $2.11\cdot 10^{-14}$, the approximation error

of $f^t(z)$ is smallest for all times t when $m = 72$ and $\ell = 2$ (cf. Tab. 1).

The poles were optimized for the rational Arnoldi approximation of order $m = 24$ (cf. Tab. 1). The dashed black line denotes the error level guaranteed by (21) in combination with Table 1. By construction of our optimized poles, all error curves are below this error level when the approximation order is 24 (even a bit earlier, although this is not guaranteed by our error bound). We note that in the case of one cyclically repeated pole (top row), the guaranteed accuracy as given in Table 1 is at a level which is larger than the initial error, so that in these cases all error curves lie entirely below this level. This is a consequence of plotting (scaled) absolute errors, since the approximated field quantities are very small. Figure 3 shows the same plots with poles optimized for $m = 36$. Here the guaranteed error is lower than the initial error also for the case of a single cyclically repeated pole.

As one can observe from Table 1, using $\ell = 3$ (or $\ell = 4$) poles does not result in further error decrease compared to using only $\ell = 2$ cyclically repeated poles. However, using a higher number of cyclically repeated poles offers more potential for parallel factorization of the shifted matrices as mentioned in Section 1. In a first level of parallelization, each of the ℓ Cholesky factorizations in Line 2 of Algorithm 1 may be carried out concurrently by a different processing unit. Further parallelization within each factorization is, of course, also possible.

For the purpose of comparison a frequency domain-based solution was computed in addition to the time domain approximation. To eliminate the effect of the error due to the rational Arnoldi approximation in the frequency domain solution, we computed the latter directly, i.e., solved the full discrete system, at all frequencies required by the FHT in order to obtain a sufficiently accurate transient. In the following, we refer to this approximation as the *brute-force frequency domain solution*, which differs from the analytical solution only by the finite element discretization error. Figure 4 shows, for a first-order Nédélec discretization, a comparison of the accuracy of the transient $\partial_t b_z(t)$ evaluated at $\boldsymbol{x} = (100, 0, 0)$ obtained for a rational Arnoldi approximation of order $m = 12$ (left column) and $m = 24$ (right column) based on one, two and three cyclically repeated poles (rows one, two and three), against the analytical solution (black line) and the brute-force frequency domain approximation (green line). For times greater than $t \approx 2 \cdot 10^{-6}$ s, it can be observed that an approximation essentially indistinguishable from the brute-force approximation is achieved already for $m = 12$. For $m = 24$ there is little or no visual difference between all solutions. The difference to the analytical solution is due to the spatial discretization error, which is improved in the analogous plots in Fig. 5 for a second-order Nédélec discretization based on the same mesh.

Fig. 6 shows the absolute error between the transient $\partial_t b_z^{(m)}(t)$ extracted from rational Arnoldi approximations of orders $m = 12, 24, \ldots, 72$ and the analytical transient solution against time for first (left column) and second (right column) order Nédélec discretization at a fixed spatial point $\boldsymbol{x} = (100, 0, 0)$ m. It can be observed that, except for the lowest-order rational Arnoldi approximation with $m = 12$, all transient errors are essentially identical, which indicates that discretization error dominates the total error in these cases. Slight differences can be observed at late times for the second-order Nédélec discretization (right column), where higher order rational Arnoldi approximations achieve a somewhat lower absolute error.

A summary of run times is given in Fig. 7, where we observe the quadratic dependence on the rational Arnoldi approximation order m with a higher constant for quadratic Nédélec elements.

For the construction of the rational Krylov basis $\mathbf{V}_{m+1}$ we have used $\ell = 1, 2, 3$ poles which have been repeated $1, 2, \ldots, 6$ times, thus yielding rational Arnoldi approximations of order $m = 12, 24, \ldots, 72$. The appropriate poles are listed in Tab. 1. The numerical effort is dominated by the number of Cholesky factorizations necessary (one for each pole), and one additional factorization[†] for the evaluation of the vector $\mathbf{b} = \mathbf{M}^{-1}\mathbf{q}$. Even though a linear system has to be solved in each rational Arnoldi iteration, the cyclic repetition of the poles yields remarkable savings in computation time (Tab. 2).

[Table 2 about here.]

[Figure 1 about here.]

[Figure 2 about here.]

[Figure 3 about here.]

[Figure 4 about here.]

[Figure 5 about here.]

[Figure 6 about here.]

[Figure 7 about here.]

5.2 Homogeneous Subsurface with Topography

As outlined above, our proposed pole selection method yields rational Arnoldi approximations which exhibit a uniform convergence that is independent of the properties of the underlying spatial discretization and conductivity distribution. Therefore, it seems attractive to include the air layer in the computational domain, which allows for the modeling of topography. The use of finite elements for the spatial discretization further adds to this benefit, as it allows for greater flexibility in approximating a curved air-Earth interface. We demonstrate this by computing transients generated by a vertical magnetic dipole source laid out atop a homogeneous half-space in the vicinity of a morphological hill-shaped feature. The interface between the air and the conducting half-space shows a moderate morphology accentuated at the center of the plane $z = 0$ around $x = y = 0$ m. The hill has a height of 38 m and a circular shape with a diameter of approximately 200 m (Fig. 8). At large distance from the hill, the interface between air and Earth is a horizontal plane aligned with $z = 0$. Fig. 8 shows the trace of the tetrahedral mesh from various azimuth and elevation angles. For the numerical experiments we have chosen Nédélec elements of order $k = 2$. The mesh consists of $28,849$ tetrahedral elements yielding $N = 181,302$ degrees of freedom.

A comparison of transients $\partial_t b_z^{(m)}(t)$ extracted from a rational Arnoldi approximation of order $m = 36$ using $\ell = 2$ cyclically repeated poles measured in the plane $y = 0$ at the points $x = [-130, 0, 130, 270]$ m and $z = [0, 38, 0, 0]$ m with an analytical solution $\partial_t b_z(t)$ obtained at the plane $z = 0$ are plotted in panels a) to d) of Fig. 9. There is no visible difference between the solution

[†] This additional factorization can be be avoided by discarding the vector $\mathbf{b}$ from the rational Krylov basis, which amounts to removing the first column of $\mathbf{V}_{m+1}$. The rational functions underlying the resulting rational Arnoldi approximants will then be of type $(m-1, m)$. Only for ease of exposition we preferred to describe and analyse our algorithm for diagonal approximants (m, m).

extracted from the rational Arnoldi approximation and the brute-force solution obtained by inverse Fourier transform of frequency-domain solutions (14). Hence, the choice of the rational Arnoldi approximation of order $m = 36$ using $\ell = 2$ cyclically repeated poles yields numerical errors which are negligible compared to the spatial discretization error.

Compared to the flat-earth response of the homogeneous half-space (black line), a distinct distortion of the transient signal $\partial_t b_z^{(m)}(t)$ is visible at early times in the vicinity of the hill (see panels a) and b) in Fig. 9), whereas at late times the response agrees well with the asymptotic behaviour of a homogeneous half-space. This is another indication that the discretization error is sufficiently small in this example.

Snapshots of the magnitude of the horizontal component of the induced electrical current system $\boldsymbol{J}$ in $\mathrm{A} \cdot \mathrm{m}^{-2}$ across the plane $y = 0$ are given in Fig. 10 for times $t = [10^{-6}, 10^{-5}, 10^{-4}]$ s.

[Table 3 about here.]

Tables 2 and 3 give a breakdown of the run times required for the different phases of the solution process for both numerical test cases. The computations were carried out in MATLAB® R2012b pinned to 8 cores of an Intel® Xeon® E5-4620 (Sandy Bridge) system (2.2 GHz). For the direct sparse linear solves we employed the PARDISO solver (Schenk and Gärtner 2004) as contained in the Intel® Math Kernel Library.

It can be observed that the computation of the rational Arnoldi approximant using formula (20) is negligible compared to the construction of the rational Krylov basis $\mathbf{V}_{m+1}$. The resulting run time is still far below the brute-force approximation in which all frequency domain solutions required for the FHT transformation to the time domain are computed by solving full finite element systems (14).

[Figure 8 about here.]

[Figure 9 about here.]

[Figure 10 about here.]

6 CONCLUSIONS

We have presented a computational method for 3-D transient electromagnetic forward modeling based on Nédélec finite element discretization in space and rational Krylov approximation for the time integration. Once the finite element discretization in space is given, the method requires only the selection of a small number of cyclically repeated poles which parametrize the rational Arnoldi method. These poles can be obtained from Table 1 depending on the desired accuracy or, if sparse direct solvers are to be employed for the finite element systems in parallel, on the available level of parallelism. The attractive main feature of our rational Arnoldi approach is the uniform accuracy in time independent of spatial mesh width or conductivity structure. Moreover, the cyclic reuse of a small number of poles allows the amortization of a small number of matrix factorizations over the generation of the rational Krylov basis. This represents an advantage over previously proposed pole sequences which are not mesh independent and require a new matrix factorization at every rational Krylov iteration. If iterative methods are used to solve the finite element systems an added benefit is that the poles as given in Table 1 lie well separated from the origin, suggesting that the resulting shifted linear systems are well-conditioned. By expressing the time and frequency domain problems in terms of matrix functions we have emphasized both the relationship of the two formulations as well as how both can be solved using rational Krylov approximation.

References

Beckermann, B. and Reichel, L. (2009). Error estimation and evaluation of matrix functions via the Faber transform. *SIAM J. Numer. Anal.* **47**, 3849–3883.

Beckermann, B., Güttel, S., and Vandebril, R. (2010). On the convergence of rational Ritz values. *SIAM J. Matrix Anal. Appl.* **31**, 1740–1774.

Beckermann, B. and Güttel, S. (2012). Superlinear convergence of the rational Arnoldi method for the approximation of matrix functions. *Numerische Mathematik* **121**(2), 205–236.

Berljafa, M. and Güttel, S. (2014). *A Rational Krylov Toolbox for MATLAB*. MIMS EPrint 2014.56. School of Mathematics, The University of Manchester, UK, page 9.

Börner, R.-U., Ernst, O. G., and Spitzer, K. (2008). Fast 3D simulation of transient electromagnetic fields by model reduction in the frequency domain using Krylov subspace projection. *Geophys. J. Int.* **173**, 766–780.

Christensen, N. B. (1990). Optimized Fast Hankel Transform Filters. *Geophysical Prospecting* **38**, 545–568.

Commer, M. and Newman, G. (2004). A parallel finite-difference approach for 3D transient electromagnetic modeling with galvanic sources. *Geophysics* **69**(5), 1192–1202. URL: `http://link.aip.org/link/?GPY/69/1192/1`.

Druskin, V. L., Knizhnerman, L. A., and Zaslavsky, M. (2009). Solution of large scale evolutionary problems using rational Krylov subspaces with optimized shifts. *SIAM J. Sci. Comput.* **31**, 3760–3780.

Druskin, V. and Zaslavsky, M. (2011). On convergence of Krylov subspace approximations of time-invariant self-adjoint dynamical systems. *Linear Algebra Appl.*

Druskin, V., Lieberman, C., and Zaslavsky, M. (2010). On Adaptive Choice of Shifts in Rational Krylov Subspace Reduction of Evolutionary Problems. *SIAM J. Sci. Comput.* **32**(5), 2485–2496.

Druskin, V., Remis, R., and Zaslavsky, M. (2014). An Extended Krylov Subspace Model-Order Reduction Technique to Simulate Wave Propagation in Unbounded Domains. *arXiv preprint arXiv:1402.7090*.

Druskin, V. L. and Knizhnerman, L. A. (1988). Spectral Differential-Difference Method for Numeric Solution of Three-Dimensional Nonstationary Problems of Electric Prospecting. *Izvestiya, Earth Physics* **24**(8), 641–648.

— (1994). Spectral approach to solving three-dimensional Maxwell's diffusion equations in the time and frequency domains. *Radio Science* **29**(4), 937–953.

Druskin, V. L. and Simoncini, V. (2011). Adaptive Rational Krylov Spaces for Large-Scale Dynamical Systems. *Systems & Control Letters* **60**, 546–560.

Druskin, V. L., Knizhnerman, L. A., and Lee, P. (1999). New Spectral Lanczos Decomposition Method for Induction Modeling in Arbitrary 3-D Geometry. *Geophysics* **64**(3), 701–706.

DuFort, E. C. and Frankel, S. P. (1953). Stability conditions in the numerical treatment of parabolic differential equations. *Math. tables and other aids to comput. (former title of Math. Comput.)* **7**, 135–152.

Ericsson, T. (1990). *Computing functions of matrices using Krylov subspace methods*. Technical report. Department of Computer Science, Chalmers University of Technology and the University of Göteborg.

Eshof, J. and Hochbruck, M. (2006). Preconditioning Lanczos approximations to the matrix exponential. English. *SIAM J. Sci. Comput.* **27**, 1438–1457. DOI: 10.1137/040605461.

Goldman, M. and Stoyer, C. (1983). Finite-difference calculations of the transient field of an axially symmetric earth for vertical magnetic dipole excitation. *Geophysics* **48**, 953–963.

Goldman, Y., Hubans, C., Nicoletis, S., and Spitz, S. (1986). A finite-element solution for the transient electromagnetic response of an arbitrary two-dimensional resistivity distribution. *Geophysics* **51**, 1450–1461.

Goldman, Y., Joly, P., and Kern, M. (1989). The Electric Field in the Conductive Half Space as a Model in Mining and Petroleum Engineering. *Math. Meth. Appl. Sci.* **11**, 373–401.

Golub, G. H. and Van Loan, C. F. (1996). Matrix Computations. 3rd. Baltimore, MD: Johns Hopkins University Press.

Gopalakrishnan, J., Garcia-Castillo, L. E., and Demkowicz, L. F. (2005). Nédélec Elements in Affine Coordinates. *Computers and Mathematics with Applications* **49**, 1285–1294.

Güttel, S. (2010). "Rational Krylov Methods for Operator Functions". PhD thesis. TU Bergakademie Freiberg.

— (2013). Rational Krylov approximation of matrix functions: Numerical methods and optimal pole selection. *GAMM Mitt.* **36**(1), 8–31.

Haber, E., Ascher, U., Oldenburg, D. W., et al. (2002). 3D forward modelling of time domain electromagnetic data. *2002 SEG Annual Meeting*. Society of Exploration Geophysicists.

Hale, T. A. D. N. and L. N. Trefethen, e. (2014). Chebfun Guide. Pafnuty Publications, Oxford.

Johansen, H. K. and Sørensen, K. (1979). Fast Hankel Transforms. *Geophysical Prospecting* **27**(4), 876–901.

Kirby, R. C. (2014). Low-Complexity Finite Element Algorithms for the De Rham Complex on Simplices. *SIAM J. Sci. Comput.* **36**(2), A846–A868.

Knizhnerman, L. A., Druskin, V. L., and Zaslavsky, M. (2009). On optimal convergence rate of the rational Krylov subspace reduction for electromagnetic problems in unbounded domains. *SIAM J. Numer. Anal.* **47**, 953–971.

Meinardus, G. and Schumaker, L. L. (1967). Approximation of functions: Theory and numerical methods. Springer.

Monk, P. (2003). Finite Element Methods for Maxwell's Equations. Oxford University Press.

Mulder, W. A., Wirianto, M., and Slob, E. C. (2008). Time-domain modeling of electromagnetic diffusion with a frequency-domain code. *Geophysics* **73**(1), F1–F8.

Newman, G. A., Hohmann, G. W., and Anderson, W. L. (1986). Transient electromagnetic response of a three-dimensional body in a layered earth. *Geophysics* **51**, 1608–1627.

Oristaglio, M. L. and Hohmann, G. W. (1984). Diffusion of electromagnetic fields into a two-dimensional earth: A finite-difference approach. *Geophysics* **49**, 870–894.

Ruhe, A. (1994). Rational Krylov algorithms for nonsymmetric eigenvalue problems. *IMA Vol. Math. Appl.* **60**, 149–164.

Saad, Y. (1992). Analysis of Some Krylov Subspace Approximations to the Exponential Operator. *SIAM J. Numer. Anal.* **29**, 209–228.

Saad, Y. and Vorst, H. (2000). Iterative solution of linear systems in the 20th century. *J. Comput. Appl. Math.* **123**, 1–33. ISSN: 0377-0427. DOI: DOI : 10 . 1016 / S0377 - 0427(00) 00412 - X. URL: http : / / www . sciencedirect . com / science / article / B6TYH - 41H9NJX - 2 / 2 / 235bc014228315f21059108e5cef9940.

Schenk, O. and Gärtner, K. (2004). Solving Unsymmetric Sparse Systems of Linear Equations with PARDISO. *Future Gener. Comp. Systems* **20**, 475–487.

Taflove, A. (1995). Computational Electrodynamics: The Finite-Difference Time-Domain Method. Norwood, MA: Artech House.

Wang, T. and Hohmann, G. W. (1993). A finite-difference, time-domain solution for three-dimensional electromagnetic modelling. *Geophysics* **58**(6), 797–809.

Ward, S. H. and Hohmann, G. W. (1987). "Electromagnetic Theory for Geophysical Applications". *Electromagnetic Methods in Applied Geophysics*. Edited by M. N. Nabighian. Volume 1. Soc. Expl. Geophys. Chapter 4, pages 131–311.

Yee, K. S. (1966). Numerical solution of initial boundary value problems involving Maxwell's equations in isotropic media. *IEEE Trans. Antennas Propag.* **AP-14**, 302–307.

Zaslavsky, M., Druskin, V. L., and Knizhnerman, L. A. (2011). Solution of 3D time-domain electromagnetic problems using optimal subspace projection. *Geophysics* **76**(6), F339–F3351.

LIST OF FIGURES

(a)

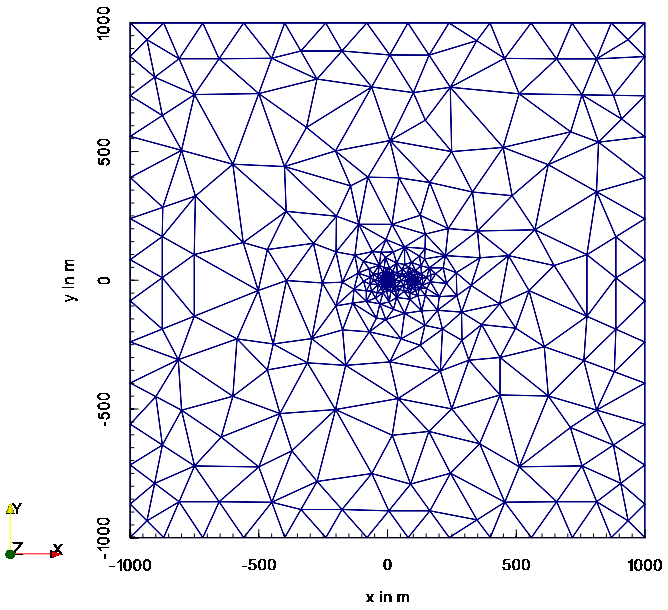

(b)

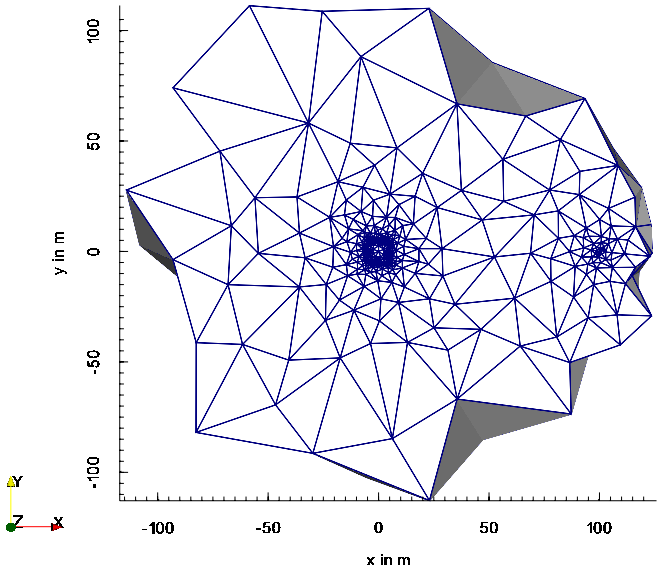

Figure 1. Trace of the tetrahedral finite element mesh used for the layered half-space model on the plane $z = 0$ (air-earth interface). Panel (a): View of computational domain from above. Panel (b): Zoom into the area containing transmitter and receiver.

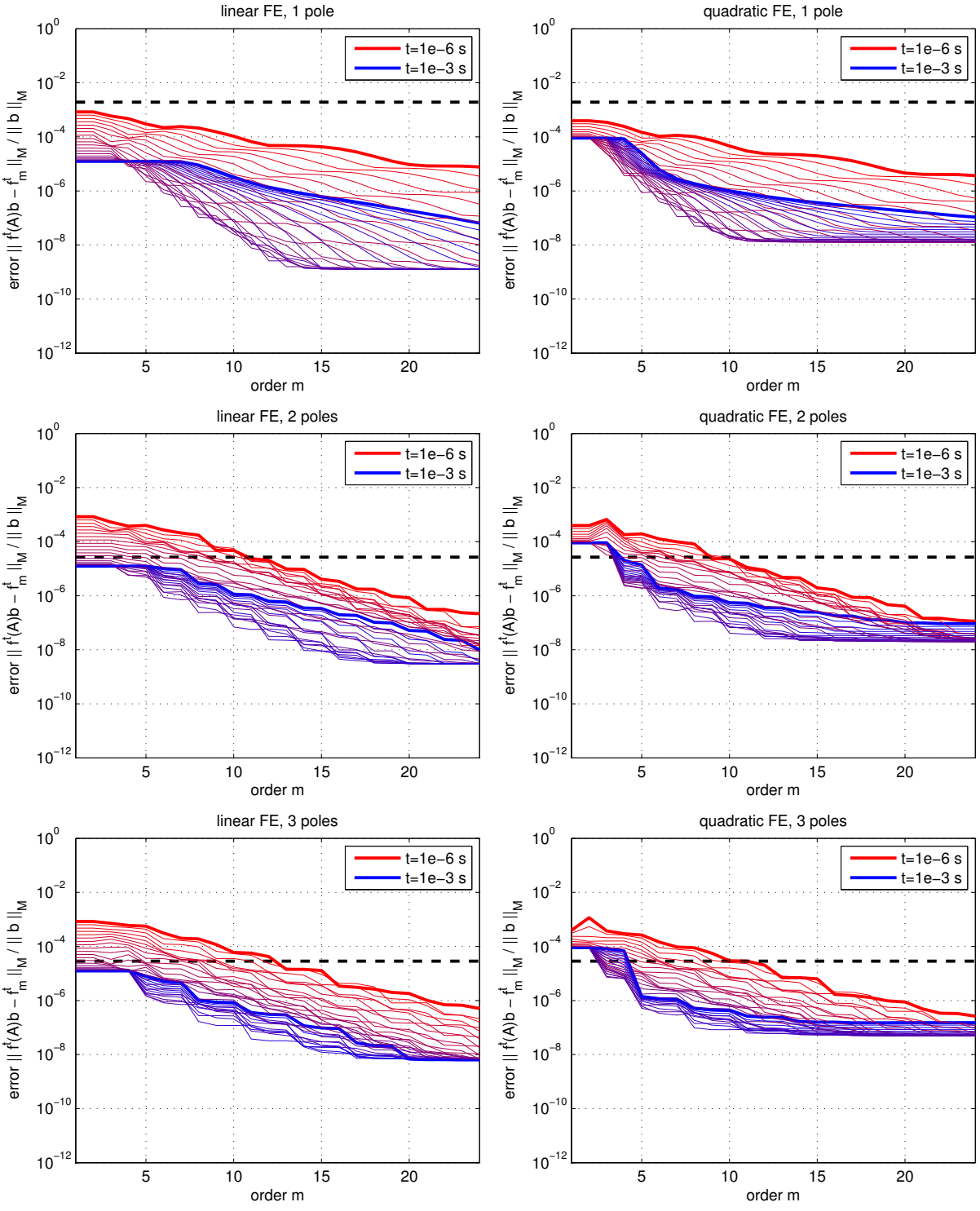

Figure 2. Scaled absolute errors of the rational Arnoldi approximations (eq. (22)) of orders $m = 1, 2, \ldots, 24$ for $\ell = 1, 2, 3$ with respect to a higher-order rational Arnoldi approximation ($m = 72, \ell = 2$) for all desired times $t \in [10^{-6} \ldots 10^{-3}]$ s, where the poles used are those optimized for $m = 24$. The dashed lines indicate the guaranteed uniform Arnoldi approximation error after $m = 24$ iterations; cf. Tab. 1 and the error bound (21).

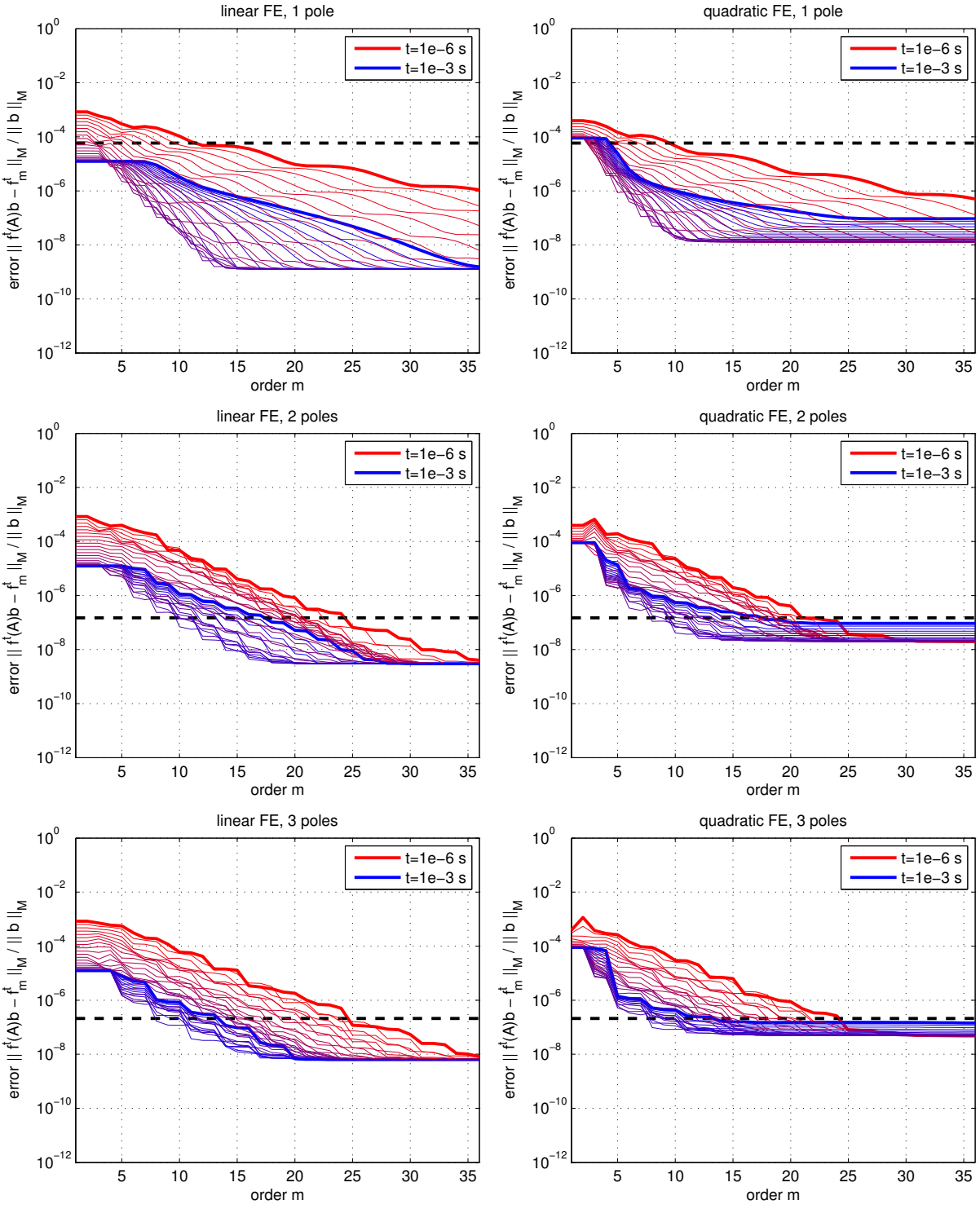

Figure 3. Scaled absolute errors of the rational Arnoldi approximations (eq. (22)) of orders $m = 1, 2, \ldots, 36$ for $\ell = 1, 2, 3$ with respect to a higher-order rational Arnoldi approximation ($m = 72, \ell = 2$) for all desired times $t \in [10^{-6} \ldots 10^{-3}]$ s, where the poles used are those optimized for $m = 36$. The dashed lines indicate the guaranteed uniform Arnoldi approximation error after $m = 24$ iterations; cf. Tab. 1 and the error bound (21).

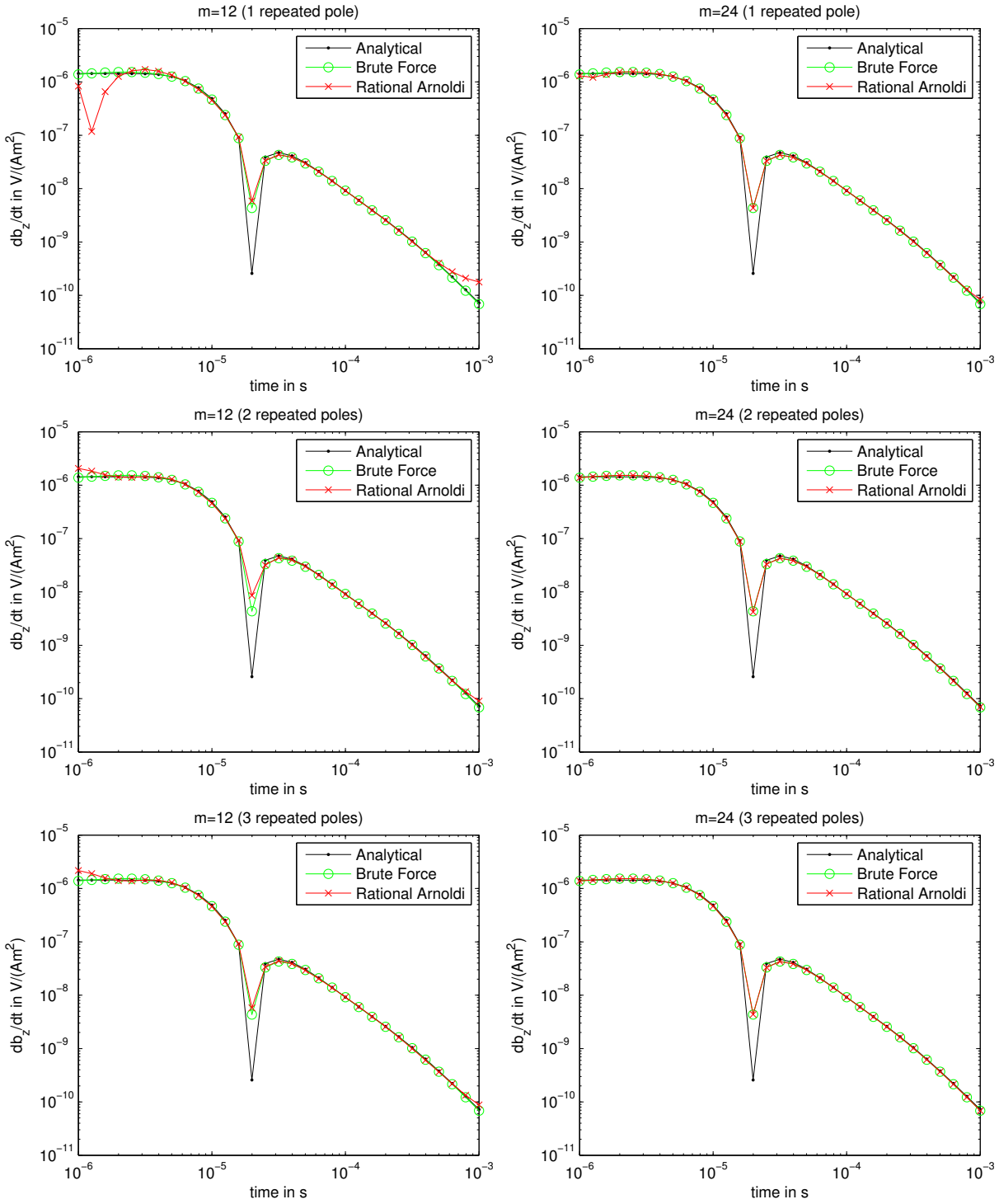

Figure 4. Layered half-space model, first-order Nédélec elements: Comparison of transients $\partial_t b_z(t)$ evaluated at $\boldsymbol{x} = (100, 0, 0)$ m obtained from the analytical solution (black), the "brute-force" solution (green) obtained by inverse Fourier transform of the frequency-domain solutions (14), and rational Arnoldi approximation (red) of order $m = 12$ and $m = 24$ (left and right columns) using $\ell = 1, 2, 3$ cyclically repeated poles (top, middle, and bottom row).

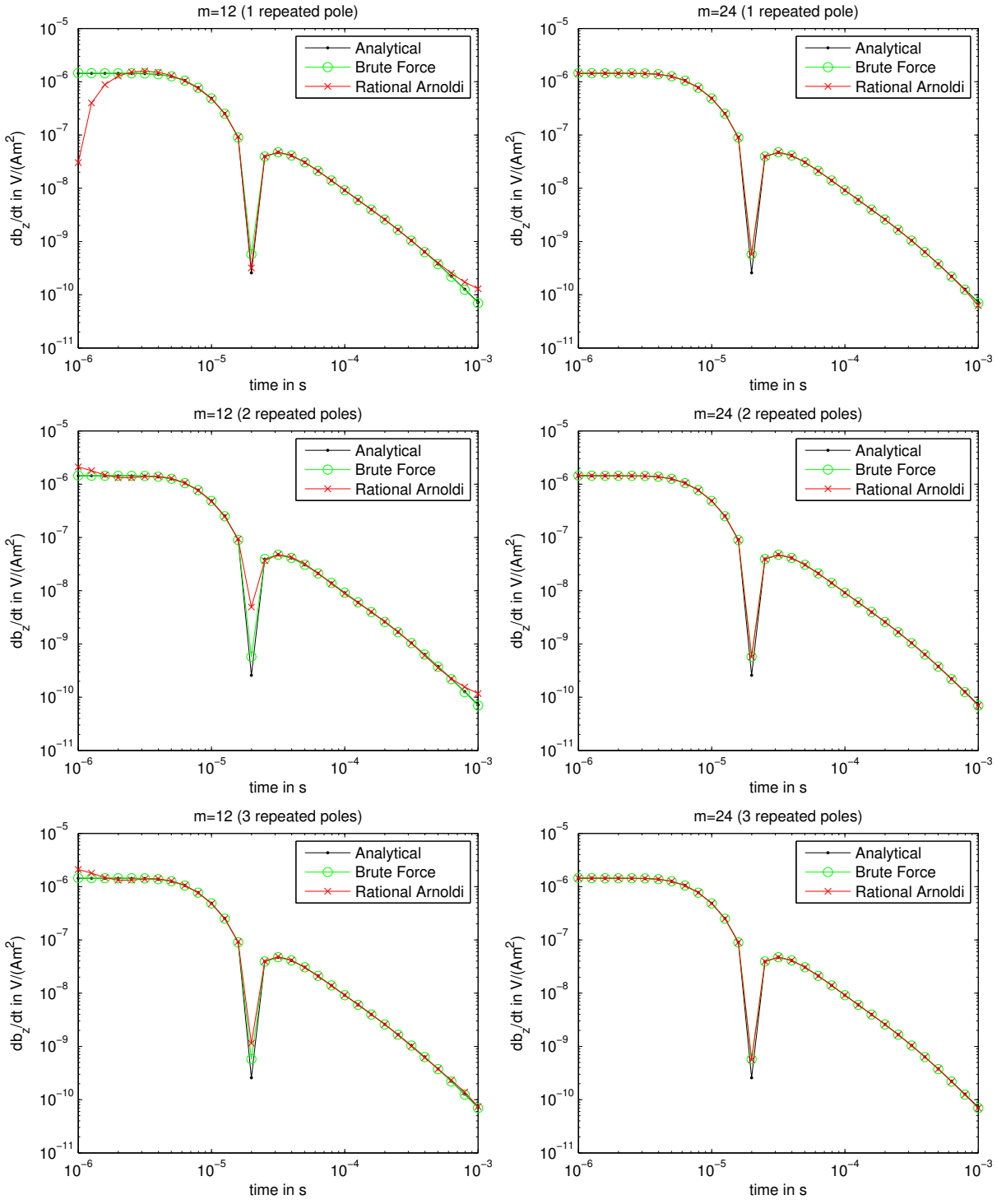

Figure 5. Layered half-space model, second-order Nédélec elements: Comparison of transients $\partial_t b_z(t)$ evaluated at $\boldsymbol{x} = (100, 0, 0)$ m obtained from the analytical solution (black), the "brute-force" solution (green) obtained by inverse Fourier transform of the frequency-domain solutions (14), and rational Arnoldi approximation (red) of order $m = 12$ and $m = 24$ (left and right columns) using $\ell = 1, 2, 3$ cyclically repeated poles (top, middle, and bottom row).

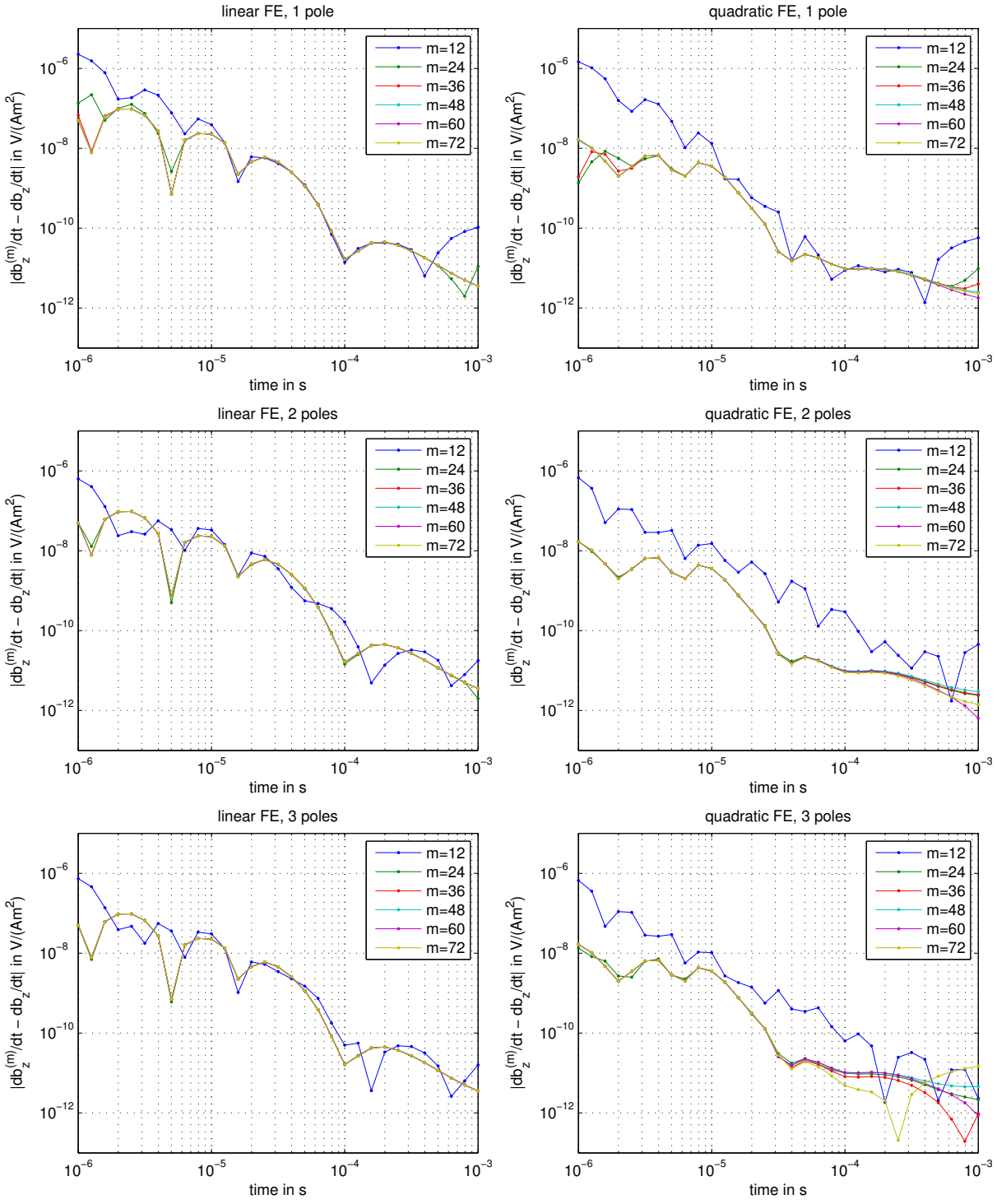

Figure 6. Absolute error of the approximate transient $\partial_t b_z^{(m)}(t)$ evaluated at $\boldsymbol{x} = (100, 0, 0)$ m extracted from rational Arnoldi approximations of order $m = 12, 24, \ldots, 72$ using $\ell = 1, 2, 3$ cyclically repeated poles compared with the transient $\partial_t b_z(t)$ obtained from the analytical solution for the layered half-space.

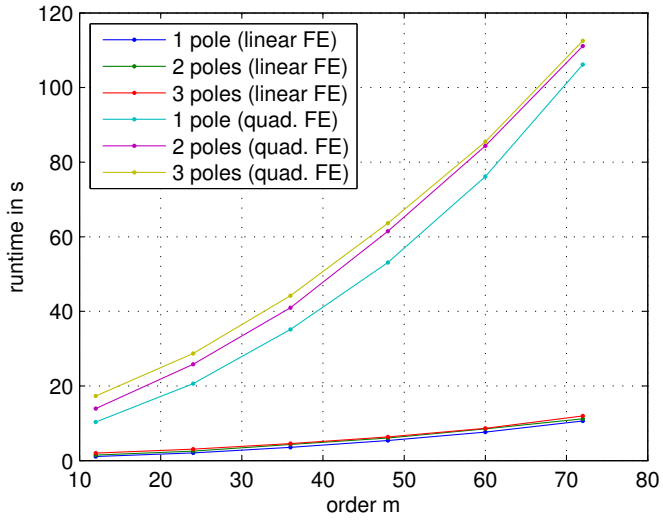

Figure 7. Plot of run times in seconds required to obtain a rational Arnoldi approximation of order $m = 12, 24, \ldots, 72$ for linear and quadratic Nédélec elements and $\ell = 1, 2, 3$ cyclically repeated poles.

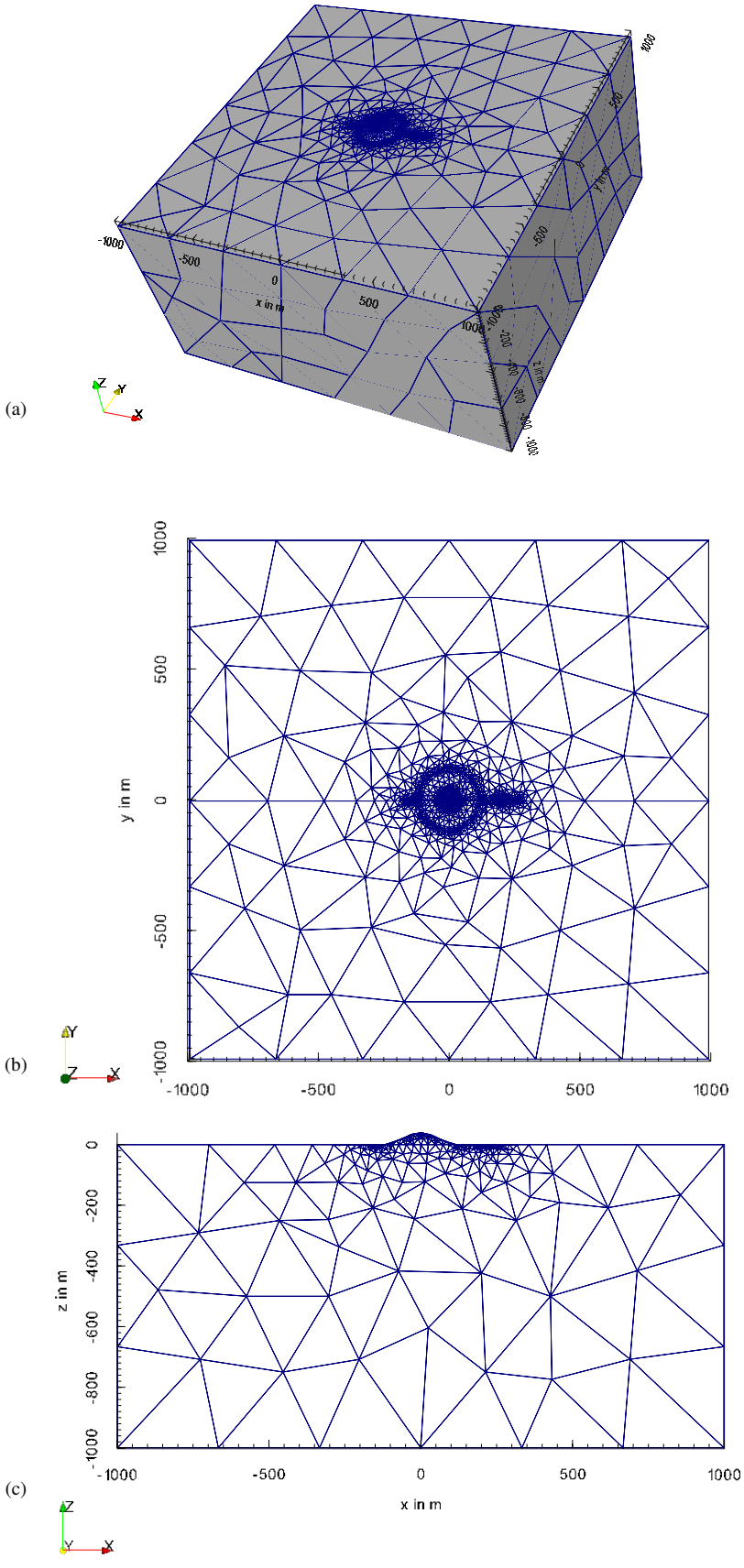

Figure 8. Trace of the tetrahedral finite element mesh used for model with topography. Panel (a): Perspective view. Panel (b): View from above the air-earth interface. Panel (c): Vertical slice along the plane $y = 0$. The air layer, which has a thickness of 1000 m, has been omitted in all pictures.

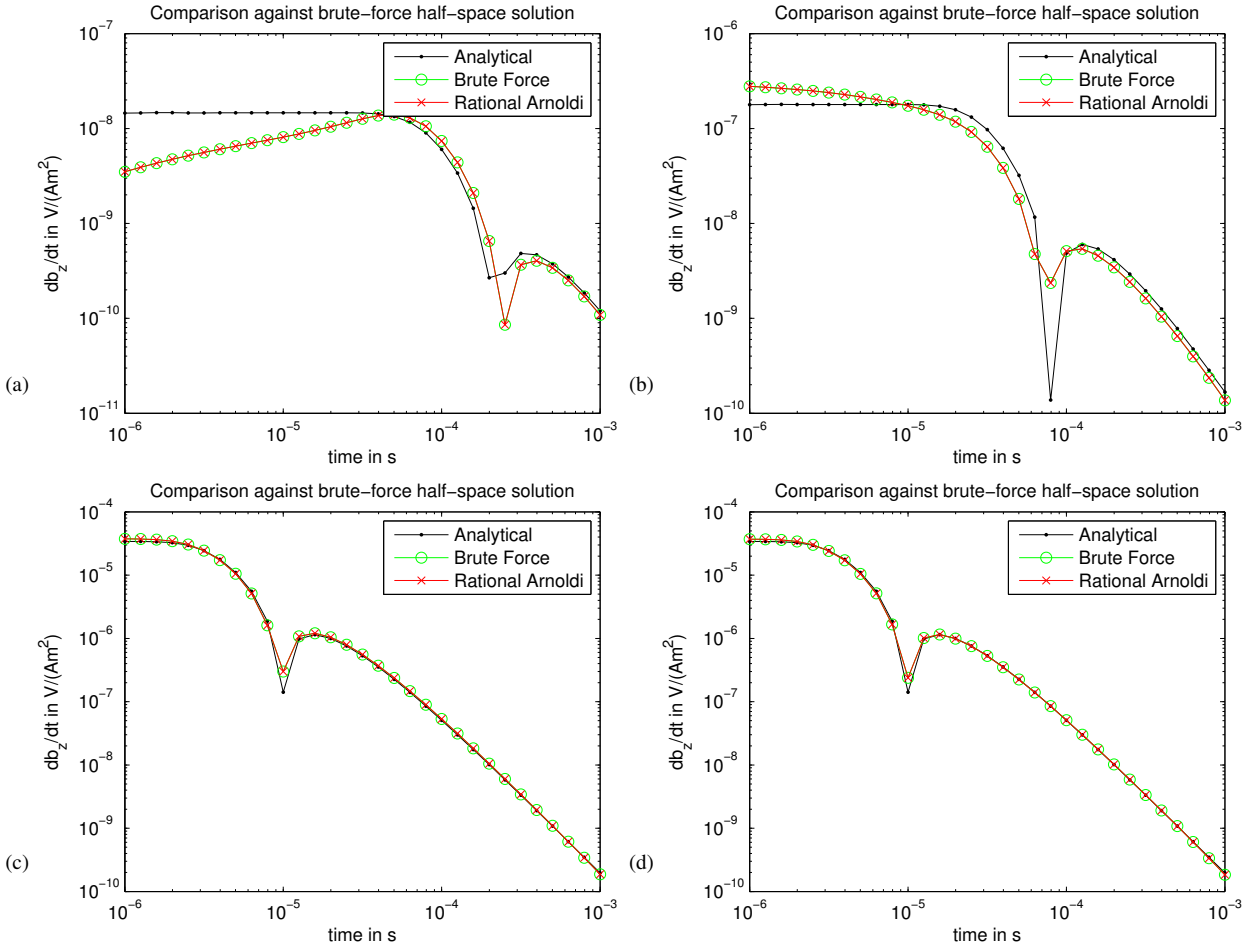

Figure 9. Topography model, comparison of transients $\partial_t b_z(t)$ at four different locations: Rational Arnoldi approximation of order $m = 36$ (red), analytical solution for flat homogeneous half-space (black) and brute-force solution obtained by inverse Fourier transform of frequency-domain solutions (green). Panels (a)-(d) correspond to the four evaluation locations $\boldsymbol{x} = (-130, 0, 0)$ m, $\boldsymbol{x} = (0, 0, 38)$ m, $\boldsymbol{x} = (130, 0, 0)$ m and $\boldsymbol{x} = (270, 0, 0)$ m, respectively. The 20×20 m^2 transmitter loop source is centered at $\boldsymbol{x} = (200, 0, 0)$ m. The spatial discretization uses Nédélec elements of order $k = 2$.

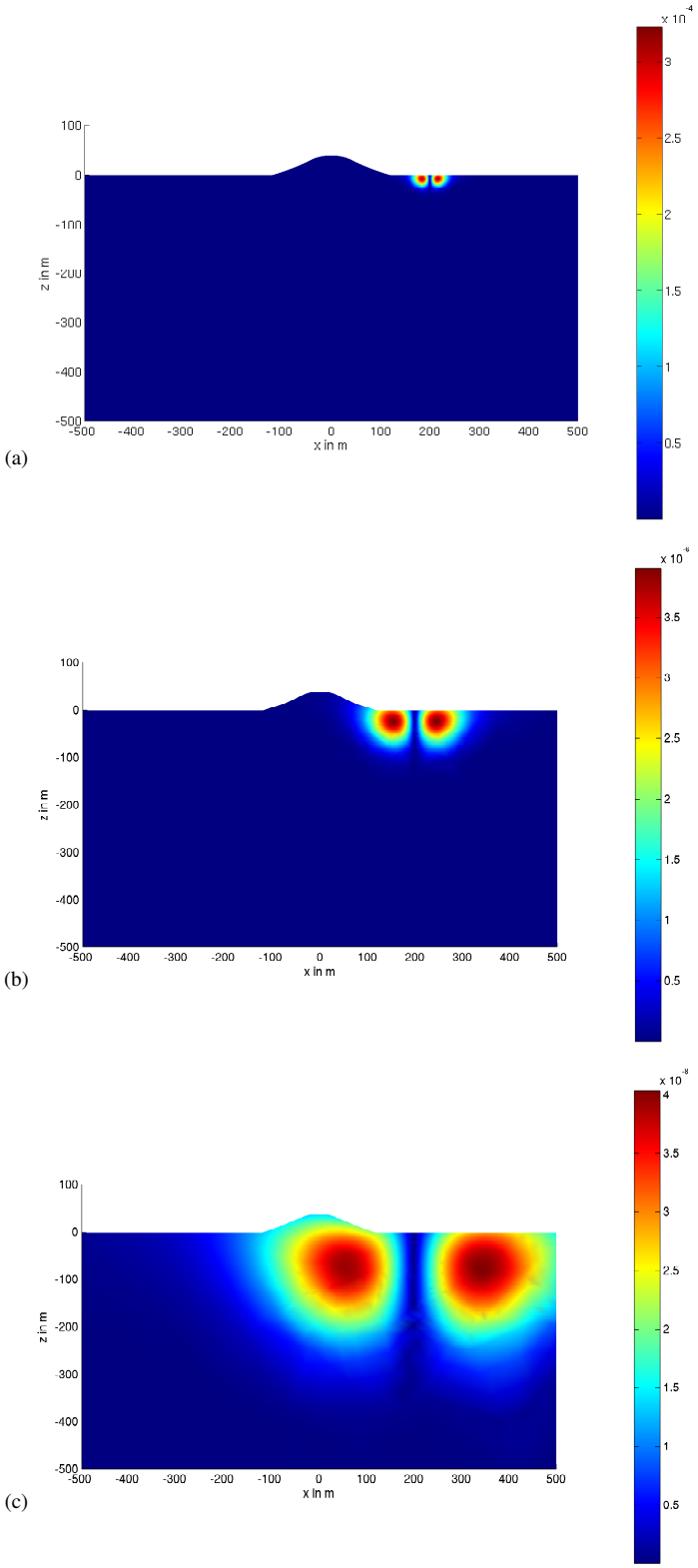

Figure 10. Topography model: Snapshots of the induced current system given in A/m^2 at times $t = [10^{-6}, 10^{-5}, 10^{-4}]$ s taken at the plane $y = 0$.

LIST OF TABLES

Table 1. Table of parameters for building a rational Krylov space for approximating $f^t(z) = \exp(-tz)$ for all $t \in [10^{-6}, 10^{-3}]$ and $z \in [0, \infty]$. The column on the left corresponds to the number of rational Krylov iterations (the dimension of the rational Krylov space minus 1). Each cell gives (an approximation for) the achievable uniform approximation error of $f^t(z)$ for all t and z, with the required cyclically repeated poles $\xi_1, \ldots, \xi_\ell$ shown in brackets. By (21) the rational Arnoldi error is bounded by twice the uniform approximation error.

m	error ($\ell = 1$ repeated pole)	error ($\ell = 2$ repeated poles)	error ($\ell = 3$ repeated poles)
12	1.71e-02 (-5.66e+04)	2.39e-03 (-1.26e+04, -7.88e+05)	2.39e-03 (-8.17e+03, -1.70e+05, -9.99e+05)
24	9.64e-04 (-1.13e+05)	1.33e-05 (-2.52e+04, -2.56e+06)	1.42e-05 (-8.36e+03, -2.41e+05, -5.23e+06)
36	2.94e-05 (-1.57e+05)	7.45e-08 (-3.32e+04, -3.88e+06)	1.05e-07 (-1.27e+04, -3.76e+05, -6.95e+06)
48	2.00e-06 (-2.14e+05)	4.87e-10 (-4.59e+04, -5.00e+06)	8.86e-10 (-2.06e+04, -4.23e+05, -1.23e+07)
60	1.02e-07 (-2.69e+05)	2.63e-12 (-5.40e+04, -6.30e+06)	6.88e-12 (-2.60e+04, -5.34e+05, -1.38e+07)
72	3.82e-09 (-3.14e+05)	2.11e-14 (-6.35e+04, -7.58e+06)	5.66e-14 (-2.60e+04, -6.73e+05, -1.96e+07)

m	error ($\ell = 4$ repeated poles)
12	2.29e-03 (-7.04e+03, -3.35e+04, -7.61e+05, -7.61e+05)
24	1.21e-05 (-1.04e+04, -4.08e+04, -1.37e+06, -5.36e+06)
36	6.74e-08 (-2.76e+04, -4.08e+04, -2.45e+06, -6.51e+06)
48	5.08e-10 (-2.76e+04, -6.02e+04, -2.98e+06, -9.62e+06)
60	2.85e-12 (-4.08e+04, -7.32e+04, -4.41e+06, -9.62e+06)
72	2.23e-14 (-3.35e+04, -1.08e+05, -5.36e+06, -1.17e+07)

Table 2. Summary of runtimes for the layered half-space model consisting of 24,582 tetrahedra.

Nédélec order	$k = 1$	$k = 2$
Problem size	$N = 27,623$	$N = 152,078$
Brute-force solution	66.36 s	739.14 s
Construction of rational Krylov basis for $m = 24$ and $\ell = 3$	3.0 s	28.7 s
Evaluation of formula (20)	0.05 s	0.08 s

Table 3. Summary of runtimes for the topography model consisting of 28,849 tetrahedra.

Nédélec order	$k = 2$
Problem size	$N = 181,302$
Brute-force solution	899.4 s
Construction of rational Krylov basis for $m = 36$ and $\ell = 3$	44.86 s
Evaluation of formula (20)	0.09 s